# Deciphering tidal signature in a fluvial-dominated delta using digital outcrop models (Roda Sandstone, Eocene, South Pyrenean Basin)

Perrine Mas, Raphaël Bourillot, Rémy Deschamps, Benjamin Brigaud, Bertrand Saint-Bezar, Philippe Razin, Eric Portier, Adrien Henry, Baptiste Hersant

**Deciphering tidal signature in a fluvial-dominated delta using digital outcrop models (Roda Sandstone, Eocene, South Pyrenean Basin)**

Perrine Mas[1,2,*], Raphaël Bourillot[2], Rémy Deschamps[3], Benjamin Brigaud[1,4], Bertrand Saint-Bezar[1], Phillipe Razin[2], Eric Portier[5], Adrien Henry[2,6], Baptiste Hersant[2]

[1] Université Paris-Saclay, CNRS, GEOPS, Orsay, France

[2] Univ. Bordeaux, CNRS, Bordeaux INP, EPOC, Pessac, France

[3] IFP Energies Nouvelles, Rueil-Malmaison, France

[4] Institut universitaire de France (IUF), Paris, France

[5] 45-8 Energy, Lyon, France

[6] LIENSs, La Rochelle Université, La Rochelle France

* corresponding author email address: perrine.mas.pro@outlook.fr, ENSEGID, Univ. Bordeaux, CNRS, Bordeaux INP, EPOC, 1 allée Fernand Daguin, 33600 Pessac, France



## Abstract

Deltaic environments are crucial depositional systems for georesources, often studied for their excellent reservoir quality in both ancient and modern contexts. However, while mixed river tide-influenced deltas are complex and important, they remain underexplored in the ancient sedimentary record. This study focuses on the Roda Sandstone, a Lower Eocene fluvial-dominated, tide-influenced delta system in the Graus-Tremp foreland basin, to address gaps in understanding the interaction between fluvial and tidal processes within these environments. Fieldwork and core analysis were conducted to investigate the Roda Sandstone. Nineteen sedimentological sections were logged, and palaeocurrents were measured in the field. A Digital Outcrop Model (DOM) was created using 11,000 drone-captured images, georeferenced with DGPS data. The Digital Outcrop Model was processed with photogrammetry and analysed using a specialised for detailed stratigraphic and facies interpretation. Additionally, five well cores, totalling 340 m, were described and integrated with the Digital Outcrop Model. The sedimentological and stratigraphic study combined with the Digital Outcrop Model interpretation led to the identification of 10 facies grouped into five facies associations and the recognising of 7 deltaic lobes, representative of fifth-order sequences. The 3D evolution of these lobes reveals variations in progradation directions and the intensity of tidal reworking. This shows a gradual shift to a tidally dominated-deflected delta front as they were prograde. This work enabled the characterization of tidal sedimentary bodies, including the dimensions of tidal dunes and bars, paleo-bathymetries, and their specific locations within both progradational and retrogradational sequences. During regressive periods, the preservation of tidal dunes and bars intercalated in the delta foresets depends on the fluvial sediment supply and autocyclic factors. Whereas the preservation of larger tidal bars on bottomsets is permitted by the lower river sediment supply during transgressive periods of fourth-order cycles. This research advances our understanding of ancient mixed deltas by providing a depositional model that clarifies the preservation of tidal features. Additionally, it underscores the value of DOMs in enhancing correlations, distinguishing different sedimentary structures generated by competing currents, and offering detailed facies mapping for improved paleoenvironmental interpretations.



Keywords: mixed delta, Roda Sandstones, reservoir analogue, Digital Outcrop Models, tidal

# Introduction

Deltaic environments are strategic depositional systems for georesources. Deltaic deposits found in ancient sedimentary records, whether outcropping or in the subsurface, are often studied for their excellent reservoir quality. Indeed, deltaic reservoirs may contain water, oil and gas or be used for gas or heat storage purposes (Tonkin, 2012). Deltas are extensively studied, and classified in qualitative and nomenclature systems that have been refined over time: seminal delta models developed a ternary classification, mainly based on modern deltas studies and their morphology along the dominant depositional process (Coleman & Wright, 1975; Galloway, 1975; Bhattacharya, 1978). They were completed by works including not only deltas but also other coastal depositional systems (e.g., beaches) (Boyd, Dalrymple and Zaitlin, 1992) or including subaqueous deltas (Zavala *et al.*, 2024). Then (Ainsworth *et al.*, 2011) extended this classification and proposed a nomenclature for complex littoral deltas that are mixed-process systems (because of the complexity revealed by studies on modern systems). However, there are few studies on mixed deltas in the ancient record, and even fewer focused on mixed river tide-influenced deltas (Willis, 2005; Steel *et al.*, 2008; Longhitano & Steel, 2017). Some reasons suggested by Willis (2005) could be, amongst others, the sometimes-unclear distinctions between estuaries and tide-dominated or tide-influenced deltas or the complex facies assemblages resulting from tidal reworking (Martinius & Van den Berg, 2011). The tidal process is a continuous phenomenon, and its sedimentary record in deltaic systems depends on fluvial activity (such as the frequency and intensity of floods, geological context, and distance from the source) (Reynaud *et al.*, 2012). Consequently, identical sedimentary structures formed by tidal currents are found in both tide-influenced deltaic systems and tidal environments (herringbone cross-bedding, tidal bundles, reactivation surfaces), which can be misleading (Bhattacharya, 1978). Some outcrops allow access to mesoscale features (e.g., tidal sand bars), which can diagnose some tidal reworking (Martinius & Van den Berg, 2011; Olariu *et al.*, 2012b).

Finally, some studies assumed that tidal influence or reworking only occurs in transgressive settings (Willis, 2005). The result is a lack of depositional models for mixed river tide-influenced deltas, leading to difficulties in identifying and integrating tidal bedforms in such delta stratigraphic framework. Moreover, bathymetry estimates are difficult to quantify in ancient systems, although they can provide valuable information for understanding their development.

The Roda Sandstone is an ancient fluvial-dominated and tide-influenced delta system deposited during the Lower Eocene in the Graus-Tremp foreland basin (Puigdefabregas *et al.*, 1985). Over the years, detailed sedimentological studies described the facies heterogeneity, depositional sequences and stratigraphic architecture of the Roda sandstones, discussing evidence of tidal influence. In addition,

work on magnetostratigraphy and palaeontology provides a very precise time constraint (Jimenez, 1987; Tosquella, 1988; Bentham & Burbank, 1996; Torricelli *et al.*, 2006). Most of these studies were done at the pluri-kilometre scale, principally using 2D cross-sections for stratigraphic reconstructions (Nijman & Nio, 1976; Nio, 1976; Puigdefabregas *et al.*, 1985; Crumeyrolle *et al.*, 1993; Crumeyrolle, 2003; López-Blanco *et al.*, 2003; Tinterri, 2007; Leren *et al.*, 2010). The depositional environment and sedimentary dynamics at the origin of sand bars have been particularly discussed due to the presence of tidal bars intercalated within delta mouth bars (Nio, 1976; Puigdefabregas *et al.*, 1985; Nio & Yang, 1991; Crumeyrolle *et al.*, 1993; Joseph, 1994). These tidal bars were the focus of a few studies that did not consider deltaic fluvial processes (Martinius, 2012; Olariu *et al.*, 2012b; Michaud & Dalrymple, 2016). The variety of signatures of sediment reworking by tidal currents within this river-dominated delta remains unclear. The stratigraphic architecture, continuity, and composition of sedimentary bodies resulting from the interaction between fluvial and tidal currents is still unclear and requires a 3D multi-scale framework, ranging from centimetre to pluri-kilometre scale.

This study proposes to combine (1) sedimentological descriptions of outcrops and of sedimentary cores drilled in the vicinity of outcrops with (2) a high-resolution (cm-scale resolution) digital outcrop model (DOM) built with georeferenced 3D drone imagery. The DOM is subsequently interpreted using field data and can be used to measure fault planes or sedimentary dips (Pringle *et al.*, 2004; Schmitz *et al.*, 2014; Deschamps *et al.*, 2017; Marques *et al.*, 2020; Tavani *et al.*, 2024). While DOMs are now widely used for geometric characterization (Enge *et al.*, 2007; Cabello *et al.*, 2018; Thomas *et al.*, 2021; Atlas *et al.*, 2023; Aliyuda *et al.*, 2024), this study also integrates facies painting directly on the DOM, using the latest developments of the Virtual Reality Geological Studio (VRGS®) software. This approach enables the documentation of sedimentary facies associations characteristic of fluvial-dominated and tide-influenced deltaic deposits in the ancient record. The kilometre scale of this study justifies the use of the DOM method, as it allows for the visualization of the entire system and facilitates zooming down to the mesoscale (centimetre resolution), offering continuous data compared to traditional methods. Additionally, we use the DOM to derive quantitative sedimentary information (such as sedimentary body dimensions, facies proportions, paleocurrent directions, and water depth estimations), which helps differentiate fluvial, tidal, and mixed sedimentary bodies (fluvial versus tidal) within the deltaic system. This method is essential for defining key characteristics that aid in their recognition.

# 1 Geological Settings

## 1.1 Regional setting

The South-Pyrenean Basin is made of an imbricated complex of Meso-Cenozoic thrust sheets that are detached over the Triassic units and overlap with southern vergence over the autochthonous Tertiary

deposits of the Ebro Basin (Puigdefàbregas & Souquet, 1986; Muñoz, 1992). This system comprises, from north to south, the Bóixols, Cotiella-Montsec, and Serres Marginals thrusts (Figure 1), interpreted as an extensional fault system inverted during the collision of the Iberian and Eurasian plates. Successive thrusting events are associated with the formation of piggyback basins. The Graus-Tremp foreland basin developed during the Montsec thrusting sequence between the Paleocene and Early Eocene (Puigdefàbregas & Souquet, 1986).

The Roda Sandstone Formation comprises shallow-marine siliciclastic deposits laterally transitioning to basin pelagic deposits over 8 km to the west (Figure 2A) (Nio & Yang, 1991; Crumeyrolle *et al.*, 1993; López-Blanco *et al.*, 2003; Leren *et al.*, 2010). This formation outcrops in the northern part of the Graus-Tremp Basin (Figure 1B) and is dated to the Ypresian based on nannoplankton and planktonic foraminifera (nannoplankton zone NP11 (Jimenez, 1987)). The Roda Sandstone is vertically bounded by shallow-marine carbonate units: La Puebla Limestone at the base and The Morillo Limestone at the top (Gozalo *et al.*, 1985). The Plateau Limestone separates the Roda Sandstone Member from the Esdolomada Member which is divided into two parts by the El Villar Limestone (Nio & Yang, 1991) (Figure 2). In some studies (Tosquella, 1988; López-Blanco *et al.*, 2003), the Lower Esdolomada Member is part of the Roda Sandstone Member, separated from the “Upper Detrital Complex” Member by the El Villar Limestone (Figure 2B).

Faults related to the regional tectonic context can be observed in the study area (Figure 2A). Initial events involve compression features in the Upper Cretaceous (Campanian), associated with the lateral ramp of the Bóixols thrust, with the Turbón thrust anticline forming as a result of this process. Maastrichtian marls cover and seal these events until the undeformed Aren Sandstones are deposited during a tectonically calm period. From the lower Paleocene to the Ypresian, differential subsidence induces the individualization of the continental limestones of the Tremp Formation to the east from the limestones of the Navarri Formation to the west, subsequently overlain by the Alveolina Limestones and algal reefs such as the Merli, Isclès and Berganuy reefs, which are located on the structural highs (Puigdefàbregas & Souquet, 1986; Serra-Kiel *et al.*, 1994). During this period, a fault known as the Merli-Congustro-Roda developed (Duguey, 1994). This fault is potentially linked at depth to the Turbón fault system, through dextral-reverse motion. The latter is visible in the field northwest of the study area (Figure 2A), at El Congustro (Duguey, 1994). Later in the Ypresian, this fault is reactivated as a sinistral-normal shear, leading to the development of normal faults arranged in "horse-tail splay" terminations (Duguey & Ott d’Estevou, 1991; Duguey, 1994). These normal faults can also be observed in the study area.

The deposition of the Roda Sandstone has been affected by synsedimentary low-amplitude folds (López Blanco, 1996; López-Blanco *et al.*, 2003) and the sediment supply is considered to have been channelled along a NNE-SSW paleovalley corresponding to the long-lived Middle Eocene–Oligocene Sis paleovalley of Eichenseer (1988) and Vincent & Elliott (1997).

## 1.2 The Roda Sandstone

The Roda Sandstone forms a world-class outcrop analogue of a deltaic reservoir (Crumeyrolle *et al.*, 1992; Crumeyrolle, 2003). Although it was recognized early on that the Roda Sandstone was deposited under the influence of tidal currents (Nijman & Nio, 1976; Nio, 1976), there has been ongoing discussion and re-evaluation of the predominant hydrodynamic agent setting. Initially, (Nijman & Nio, 1976; Nio, 1976) interpreted the Roda Sandstone as an aggrading system of tidal mouth bars (named sand waves following the ancient terminology (Allen, 1980)). On the other hand, (Puigdefabregas *et al.*, 1985) emphasized fluvial processes, describing a complex delta arrangement supplied by a braided fluvial system and reworked by tides, with ebb currents directed to the north-northwest and flood currents to the south-southeast (Figure 1B). Subsequently, (Yang & Nio, 1989; Nio & Yang, 1991) revised their interpretation and identified an ebb-dominated delta with an associated estuarine channel based on the similarities with the present-day estuary of the Eastern Scheldt mesotidal basin. The interpretation of the Roda Sandstone as a fluvial-dominated delta reworked by tidal currents was further supported by Crumeyrolle *et al.* (1993), Crumeyrolle (2003), López-Blanco *et al.* (2003), Tinterri, (2007) and Leren *et al.* (2010). Later studies by Martinius (2012) and Michaud & Dalrymple (2016) focused on tidal bars during fourth and higher-order transgressive periods, while (Olariu *et al.*, 2012b) specifically identified and studied a tidal bar in the Esdolomada Member.

The Roda Sandstone formation was divided into six sandstone bodies based on lithostratigraphic criteria (Tosquella, 1988), named from the oldest to the most recent as U to Z (Figure 3). These are vertically delimitated by limestone beds and more distally by marls deposits. Lithostratigraphically, sandbodies U to Y compose the Roda Sandstone Member of the Roda Sandstone Formation, whereas the Z sandbody is equivalent to the Lower Esdolomada Member.

In this study, we correlated the local magnetostratigraphic Roda section (Bentham & Burbank, 1996) to the geomagnetic polarity time scale from GTS 2020 (Gradstein *et al.*, 2020). The polarity inversion between chrons C24r.3r and C24n.3n at the base of the La Puebla Limestone gives an age of 53,9 Ma and the following inversion between C24n.3n and C24r.2r corresponding to the Plateau Limestone stands for an age of 53,25 Ma (Figure 3). This magnetostratigraphical data indicates an age comprised between ca. 53,75 and 53,25 Ma for the Roda Member. Based on this magnetostratigraphic data, the stack of sandbodies composing the Roda Sandstone Member is interpreted as a vertical sequence of

prograding, aggrading, then retrograding system tracts (Mutti *et al.*, 1988; Yang & Nio, 1989; Crumeyrolle *et al.*, 1993; Tinterri, 2007), within a third-order cycle (Vail *et al.*, 1975; Hardenbol *et al.*, 1998). The maximum progradation of the delta is reached with the Y sandstone body, which is the most extensive but also the one with the most complex internal architecture. The Y sandbody also appears to be affected by relative sea-level variations of higher-order cycles (fifth or sixth (Crumeyrolle *et al.*, 1993). In a study more focused on the internal architecture of the sandbodies (Joseph, 1994) divided the Y body into three, later (López-Blanco *et al.*, 2003) adopted this division and distinguished another sub-unit in the top part of Y3 that was named Y4 (Figure 3).

The Roda Sandstone composition comprises medium to coarse-grained arkose with prevailing minerals such as quartz, potassium feldspar, and plagioclase (Molenaar & Martinius, 1990; Chanvry *et al.*, 2018). An early calcite cement lithified the sandstone, locally preventing mechanical compaction and resulting in more cemented nodules associated with abandonment surfaces (Molenaar, 1990; Molenaar & Martinius, 1990; Musial, 2006). The clay fraction is relatively low, the fine grains are mostly silts, and the clay mineral assemblages are characterized by a prevalence of interlayered clays and a low proportion of kaolinite (Chanvry, 2016).

## 2 Data & Methods

Observation and data collection have been made both during fieldwork in the area of Roda de Isabena (Figure 4) and at the core repository of Boussens (STC, France). Nineteen sedimentological sections have been logged, named Codoñeras (C), Serraduy South (SS), Zipaguerne 1 and 2 (Z1 and Z2, two log sections), Puebla East (PE), El Villar (EV), El Villar South (EVS), Meander 1 to 4 (M1-4, four log sections), Road-cut (RC), Las Forcas 1 to 5 (LF 1-5, five log sections), North Road-cut (NRC) and Puebla North-West (PNW) (Figure 4). Palaeocurrents have been measured in the field in order to plot the corrected azimuth on rose charts.

For the Digital Outcrop Model (DOM), 11,000 photos have been captured using a Mavic Pro 2 (DJI®) drone equipped with a 20-megapixel resolution camera over an area of approximately 3,3 km² (roughly 2/3 of the outcropping surface of Y sandbody; Figure 4). The image resolution is about 3 cm/pixel, and two types of image sets were acquired. First, images have been captured with the drone camera pointing nearly perpendicular to the ground, with a minimal angle between 80° and 70° relative to the surface, covering the entire study area. Second, images were captured with the drone camera oriented horizontally in order to capture cliffs. Drone pictures were georeferenced using an onboard GPS, gyroscope, and accelerometer, and a Differential Global Positioning System (DGPS) campaign was conducted to measure precise (sub-decimetre) coordinates on targets placed in the field, visible on the drone photos and acting as georeferenced control points (GCPs).

Field data were supplemented by the description of 50 to 83 m long cores (for a total length of 340 m) at the core repository of Boussens along five wells (RODA 1, RODA 4, RODA 5, RODA 6, and RODA 7, Figure 4). The cores were drilled in 1989 in the frame of the ARTEP project (Elf-IFPEN) and were made available by Total Energies. These wells are located in the vicinity (from 130 to 450 m) of the outcropping Roda Sandstone (Figure 4).

Based on the image dataset, a photogrammetric model was assembled using Pix4Dmapper® software resulting in four georeferenced tiled models as Scene Layer package files (.slpk), forming four DOM. Additionally, each DOM was also exported as a triangulated mesh comprising a 3D object (.obj) and a texture file (.jpg) representing the ortho-projection of the pictures on the oriented mesh triangles. Both .slpk and .obj plus .jpg texture DOM formats were imported into the Virtual Reality Geological Studio software (VRGS®, (Hodgetts, 2010)). The triangulated mesh models were georeferenced with the VRGS® "GCP georeferencing tool" using remarkable points on the tiled model as GCPs.

With VRGS®, wells and stratigraphic sections were first located on the DOM, and their paths were digitized (Figure 5). Secondly, sedimentary structures, fault planes, and stratigraphic surfaces were manually digitized on the DOM, on the digitized wells and vertical sections. In this study, the surfaces selected as sequence boundaries are maximum regressive surfaces (MRS) due to the better expression of these surfaces (Catuneanu *et al.*, 2011), although a few maximum flooding surfaces (MFS) were identified locally.

VRGS® interpretation tools, such as thickness and dip measurements, were employed to check the correlations with the wells and expand the paleocurrents dataset. Finally, the outcrop was painted in facies using the Facies Paint tool in VRGS®, and the digitized wells and sections were interpreted in facies according to the facies classification defined from outcrops and core descriptions.

The 3D facies map was then imported into the geomodelling software Petrel® as a point cloud with attributes to quantify the different facies proportions and estimate water depths for each of them.

The following sequential pattern was used to interpret the vertical sections, the well cores and the DOMs: The interpreted units are high-frequency cycle deposits, corresponding to parasequences (Van Wagoner *et al.*, 1988) or genetic units (Busch, 1971; Guillocheau *et al.*, 2004) as they are "relatively conformable successions of genetically related beds or bedsets bounded by flooding surfaces" (Van Wagoner *et al.*, 1988). This vertical staking of parasequences approach is particularly used in coastal and shallow-water systems (Catuneanu *et al.*, 2009). The flooding surfaces are better expressed than the erosive sequence boundaries (SB) used in the depositional sequence model (Posamentier & Vail, 1988). Those erosive surfaces in the proximal part of the system are equivalent to conformable surfaces

toward the basin and become the base surface of the sand bodies on which the bottomsets of the clinoforms downlap. In contrast, Maximum Regressive Surfaces (MRS) correspond to flooding surfaces and the cease of the detrital sediment supply. They are recognized at the top of the sand bodies and are often marked by early diagenesis cementation phenomena that can act as stratigraphic reservoir heterogeneities.

# 3 Results

## 3.1 Facies analysis

Sixteen facies have been identified through outcrop analysis and core description (Table 1, Figure 6, Figure 7, Figure 8, Figure 9). These facies have been categorized based on lithology, grain size, sedimentary structures, and ichnofossils. They have been grouped into five facies associations (FA) following the geometrical subdivision of deltaic clinoforms into topset, foreset and bottomset strata (Gilbert, 1885; Barrel, 1912; Bhattacharya, 1978). The five facies associations follow a continuum from proximal to distal deltaic environments: (1) mouth bar topsets (FA 1), (2) mouth bar foresets (FA 2), (3) mouth bar bottomsets (FA 4), (4) distal mixed deposits (FA 4), and (5) pro-delta marls (FA 5). The bioturbation index was evaluated following MacEachern & Bann (2020).

| Facies association | Sedimentary facies | Description | Bioturbation Index (after MacEachern and Bann, 2020) | Interpretation |
|---|---|---|---|---|
| FA1 - Deltaic mouth bar topsets | F1a - Highly bioturbated silty to medium sandstone enriched in shells | Silty to medium-grained sandstones, highly bioturbated, sometimes oxidized, and enriched in shells (mussels, bivalves, echinoderms and gastropods), organic debris, mud clasts and presence of benthic foraminifera but no nummulites visible. Typical trace fossil assemblage of *Macaronichnus, Skolithos, Thalassinoides* and *Ophiomorpha* | 1-5 | Proximal and protected area, restricted marine domain (lagoon) with episodic flood events dominated by decantation processes. |
| | F1b - Coarse sandstone with trough cross-bedding | Poorly sorted medium to very coarse-grained sandstone with trough cross-bedding in decimetre-thick fining-up sequences; erosive base; top bed often bioturbated, enriched in shell debris and organic matter at the top; occasional carbonate cemented concretions nucleated around shell accumulations. Typical trace fossil assemblage of *Macaronichnus* and *Ophiomorpha* | 0-3 | Delta mouth bars topsets solely dominated by high energy fluvial tractive currents |
| FA2 - Deltaic mouth bar foresets | F2a - Medium sandstone with trough cross-bedding | Moderately to poorly sorted medium to coarse-grained sandstone in coarsening and thickening-up sequences; low angle bedsets; occasional trough cross-bedding; occasional carbonate cemented concretions at the top of the beds. Typical trace fossil assemblage of *Macaronichnus* and *Ophiomorpha* | 0-3 | Delta uppermost foresets on the delta front dominated by fluvial tractive currents and avalanching |
| | F2b - Medium sandstone with planar cross-bedding | Medium to coarse (locally very coarse) grained sandstones in decimetre-thick fining-up sequences with high angle tabular cross-bedding; frequent reactivation by coarser material; bioturbated at top; occasional carbonate cemented concretions nucleated around shell accumulations. Typical trace fossil assemblage of *Ophiomorpha*, *Palaeophycus* and *Cylindrichnus* | 0-3 | Delta uppermost foresets in the delta front dominated by avalanching |
| | F2c - Medium sandstone with cross- or compound-bedding | Moderately sorted medium to coarse-grained sandstones in coarsening and thickening-up sequences; decimetre to metre thick beds; compound bedding, reactivation surfaces; occasional mud drapes; tidal current directions: N310°; occasional carbonate cemented concretions nucleated around shell accumulations. Typical trace fossil assemblage of *Ophiomorpha*, *Skolithos* and *Fugichnia* | 0-4 | Middle part of the foresets in the delta front dominated both by avalanching and tidal tractive currents |
| | F2d - Massive structureless medium sandstone | Moderately to well- sorted medium to coarse-grained sandstone in structureless metre-thick bedsets, centimetre-sized wood debris and dispersed very small (millimetre-sized) shell debris; probably highly bioturbated. Typical trace fossils of *Ophiomorpha* | 1-3 | Middle part of the foresets in the delta front dominated by avalanching |
| | F2e - Coarse sandstone with sigmoidal cross-bedding | Coarse to very coarse-grained sandstones, poorly to moderately sorted; Occasional presence of micas and feldspars; Beds organized in decimetre to metre-high simple or compound dunes with sigmoidal cross-bedding, sometimes with current ripples along foresets; The bi-directionality seems preserved with possibly a few reactivation surfaces. The bedsets are either dipping NNW (≃N310°) or SSE (≃N150°). Typical trace fossil assemblage of *Ophiomorpha* and *Skolithos*. | 0-2 | Simple dunes or compound dunes part of a tidal bar Water depth is estimated to be up to 10 m (*Allen, 1980*) |

| | | | | |
|---|---|---|---|---|
| | F2f - Master bedding silty claystone | Silty claystone with lenticular to wavy bedding, occasionally current ripples; Floating quartz grains and numerous shells; Presence of leave debris, mud clasts, and ferrous nodules; quite bioturbated. Typical trace fossils of *Ophiomorpha* and *Paleophycus*. | 1-4 | Low energy tidal currents, Abandonment phase of the bar, segmenting two phases of the tidal bar. |
| FA3 - Deltaic mouth bar bottomsets | F3a - Fine sandstone with dunes | Centimetre to decimetre thick beds of fine to medium-grained sandstones; many fining-up cycles in thickening and coarsening-up sequences; dominated by current dunes, and occasional hydraulic jumps; highly bioturbated. Typical trace fossil assemblage of *Zoophycos, Ophiomorpha* and *Skolithos* | 1-4 | Bottomset beds deposited by gravity flow at the low-gradient slope of the delta |
| | F3b - Very fine sandstone with current ripples | Centimetre-thick beds of very fine to fine-grained sandstones; frequent current ripples with mud drapes; occasional mud clasts, organic matter debris, and nummulites, rare annelid tubes; sedimentation interruption surfaces; heavily bioturbated. Typical trace fossil assemblage of *Ophiomorpha*, *Thalassinoides* and *Planolites* | 1-5 | Bottomset beds deposited by gravity flow at the low-gradient slope of the delta |
| | F3c - Coarse sandstone with sigmoidal cross-bedding | Coarse to very coarse-grained sandstones, poorly to moderately sorted; Occasional presence of micas and feldspars. Beds organized in medium dunes with sigmoidal cross-bedding, reactivation surfaces, and possible current ripples along foresets; Decimetre to metre-thick bedsets are dipping NNW (≃N310°) and their thickness could be modulated by neap-spring water cycles. Typical trace fossil assemblage of *Ophiomorpha*, *Thalassinoides*, and *Rosselia*. | 0-2 | Reworked sediments on the delta front by bi-directional tidal currents forming a tidal dune or tidal bar. Water depth is estimated to be approximately 15 m (*Martinius & Van den Berg, 2011* after *Nio & Yang, 1991*) |
| | F3d - Finely laminated silty claystone | Millimetre to centimetre thick finely laminated silty claystone with occasional current ripples, lenticular or wavy bedding. Sometimes oxidized. Typical trace fossils of *Ophiomorpha* and *Thalassinoides*. | 1-4 | Clay-drape couplets in tidal bars deposited during slack-water periods. |
| FA4 - Low energy mixed distal deposits | F4a - Bioturbated medium-grained sandstone | Medium to coarse-grained, poorly sorted sandstone, with no sedimentary structure visible but heavily bioturbated. Frequent shell clasts, millimetre organic matter debris, and occasional pyrite or mud clasts. Typical trace fossil assemblage of *Ophiomorpha* and *Planolites* | 2-5 | Transition between distal delta front part to prodelta, dominated by tidal/fluvial tractive current |
| | F4b - Bioturbated fine sandstone | Silty to fine-grained dark grey or beige sandstone, with no sedimentary structure visible but heavily bioturbated. Frequent shell clasts, millimetre-sized organic matter debris, and occasional pyrite or mud clasts. Occasionally affected by loading or interrupted by coarser-grained sandstone intervals. Poorly observed in outcrop. Typical trace fossil assemblage of *Ophiomorpha, Zoophycos, Teichichnus, Palaeophycus, Siphonichnus, Skolithos, Thalassinoides, Planolites* and *Diplocraterion* | 2-5 | Transition between distal delta front part to prodelta, dominated by tidal/fluvial tractive current |
| | F4c - Nummulitic calcareous deposits | Carbonate deposits: or wackestone to grainstones/rudstones enriched in foraminifera (mostly nummulites, few alveolines, orbitolites or milioles) and millimetre to pluri-centimetre sized bioclasts (bivalves, gastropods, corals); occasionally affected by loads and highly bioturbated. Poorly observed in outcrops. Typical trace fossil assemblage of *Skolithos, Scolicia, Planolites, Siphonichnus* and *Schaubcylindrichnus* | 0-4 | Distal delta front part with relatively low sediment supply |

| | | | | |
|---|---|---|---|---|
| FA5 - Fine pro-delta deposits | F5a - Shell debris lag | Silty to shaly grey marls with numerous millimetre to centimetre-sized shell debris (bivalves, gastropods or echinoderms), sometimes in local accumulations. Dispersed nummulites and occasional pyrites or organic matter debris. Poorly observed in outcrop. | 0-2 | Prodelta part above the storm wave-base. The shell debris lags are formed during high energy episodes.<br><br>Prodelta part below storm wave level, dominated by decantation processes and hemipelagic deposits |
| | F5b - Nummulitic marls | Shaly grey marls more or less enriched in foraminifera (mostly nummulites). Occasional to rare bioclasts (bivalves, gastropods or echinoderms). Presence of organic or vegetal debris; little bioturbated. Poorly observed in outcrop. Typical trace fossils of *Palaeophycus* | 0-3 | |

*Table 1 - Overview of identified facies associations in the Roda Sandstone. Further discussion and references can be found in the main text.*

### 3.1.1 FA 1: Deltaic mouth bar topsets

*Description* - This facies association predominantly occurs in the northeastern part of the study area, representing the most proximal part of the deltaic system. It extends laterally westward to the deltaic mouth bar foresets deposits (FA 2). This facies association includes two facies: (1) Highly bioturbated silty to medium sandstone enriched in shells (F1a) and (2) coarse sandstone with trough cross-bedding (F1b).

Facies F1a comprises silty to medium-grained sandstone organized in beds with thicknesses ranging from 1 to 5 metres, including high shell content, e.g., mussels, bivalves, and gastropods (Figure 6B, Figure 6D), and without distinct sedimentary structures (Figure 6A). Facies F1b is the coarsest sandstone in the studied area. F1b is a poorly sorted, medium to very coarse sandstone organized in decimetre-thick beds with an erosive base. The upper portions of the beds in Facies F1b often display enrichment in shell debris and organic matter (Figure 6C). These beds exhibit a fining-upward trend (Figure 6C), and a very low-angle trough bedding (Figure 6E). Carbonate-cemented concretions of pluridecimetre to a metre in size can be observed locally, nucleating around accumulations of shells.

The Bioturbation Index (BI; (MacEachern & Bann, 2020)) is moderate for F1b (BI 0-3) and high for F1a (values up to 5), and the ichnofauna assemblage is dominated by *Macaronichnus* and *Ophiomorpha* in both facies, with also *Skolithos* and *Thalassinoides* for F1a.

*Interpretation* - The presence of distinct evidence of strong fluvial tractive currents suggests facies F1b was deposited in mouth bar topsets. This facies corresponds to the most proximal deposits observed in the Roda Sandstone, as the alluvial system upstream is not preserved (Puigdefàbregas & Souquet, 1986; Eichenseer, 1988). In facies F1a, the abundance of marine shells, combined with the intense bioturbation (with the absence of distal environment nummulites), indicates a relatively calm and protected environment. The presence of *Macaronichnus* suggests a protected environment associated to the proximal part of the delta (e.g., topsets) at the top of the mouth bar as it appears in intertidal and shallow subtidal deposits (MacEachern *et al.*, 2005; Knaust, 2017). Although episodic floods are possible, the primary sedimentary process is likely decantation. The water depth is then very shallow, as Macaronichnus ichnofacies is generally found in the intertidal zone (MacEachern *et al.*, 2005), and the mean tidal range is estimated to be 3,6 m (Martinius & Van den Berg, 2011).

### 3.1.2 FA 2: Deltaic mouth bar foresets

*Description* – The facies association FA 2 constitutes the predominant component of the Y sandbody at all studied locations. These deposits form plurimetre-thick (up to 15 m-thick) vertical stacks of inclined bedsets highlighting the slope of the clinoforms (Figure 7A). Four facies of medium-grained sandstone

have been identified and differentiated on the basis of their sedimentary structures: (1) decimetre-thick beds of medium sandstone with trough cross-bedding (F2a), (2) medium sandstone with planar cross-bedding (F2b), (3) medium sandstone with cross- or compound-bedding (F2c), and (4) massive structureless medium sandstone (F2d).

Facies F2a, F2b and F2c present moderately to poorly sorted (medium to coarse-grained) sandstone, forming plurimetre packages with pluridecimetre-thick beds. In all facies, the base of beds displays low-angle clinoforms with dipping azimuth comprised between N240° and N310°. In facies F2a, beds are coarsening-up (Figure 7) and show a thickening-up trend, along with trough-cross beddings dipping in the same direction as the clinoforms (Figure 7D).

Decimetre-thick fining-up sequences with high-angle tabular cross-bedding (dipping in the same direction as the clinoforms) are typical of Facies F2b (Figure 7E), with coarser material often associated with reactivation surfaces (Figure 7B). In Facies F2c, sandstones form 2-5 metres thick coarsening-up and thickening-up packages of pluridecimetre to metre-thick beds. Compound bedding is observed in Facies F2c, with occasional reactivation surfaces and sometimes mud drapes (Figure 7H). In facies F2c, the dip of cross-beddings indicates paleocurrents directed toward the northwest (between N310°-N320°), differing from the bedset directions dipping towards the southwest or west (Figure 7G).

In facies F2d, coarse-grained sandstone is moderately to well-sorted, with massive metre-thick beds. No sedimentary structures are visible, but centimetre-sized wood debris and dispersed very small (millimetre-sized) shell debris are present (Figure 7F). Carbonate concretions of pluri-decimetre to a metre in size may be locally present, usually within the upper beds. They seem to nucleate around shell accumulations.

Moreover, some coarser-grained sandstone with sigmoidal cross-bedding (F2e) forming decimetre to metre-thick simple dunes (Figure 7I) or plurimetre-thick compound dunes (Figure 7K, Figure 7M) were identified. These sand bodies are often interbedded with F2c deposits (Figure 7M). Agglomerated dunes form bars that are plurimetre-high (3-5 m, Figure 7M) and their length (measurement of their long axis) are estimated to reach hundreds of metres (Leuven *et al.*, 2016). The bi-directionnality is shown either with bedsets dipping NNW (≃N310°) or SSE (≃N150°), but also by reactivation surfaces formed by subordinate currents. Facies F2e is interbedded with silty claystone forming master bedding (i.e. the architectural plane indicating the bar accretion) on top of the bedsets (F2f, Figure 7L). These centimetre to pluridecimetre-thick interbeds show lenticular to wavy bedding, occasionally current ripples.

The bioturbation index is moderate (BI 0-4) in FA 2. Common *Ophiomorpha* trace fossils appear in all facies, including also common *Macaronichnus* for facies F2a, *Palaeophycus* for F2b and F2f, *Cylindrichnus* for F2b, *Skolithos* for F2c and F2e, and *Fugichnia* for F2c.

*Interpretation* – This facies association is interpreted as deltaic foresets deposits mainly prograded from east to west. This interpretation is based on the finer grain size compared to facies F1b, the sedimentary structures indicating a relatively high energy environment, the low bioturbation index suggesting an important sediment supply, and the clinoform geometries of the bedsets (Bhattacharya, 1978; Allen *et al.*, 1979; MacEachern *et al.*, 2005).

Facies F2a shares similarities with facies F1b but with a smaller grain size and is part of the clinoforms so it is interpreted as the uppermost part of the mouth bar foresets, still dominated by fluvial influence. Then laterally the facies F2b is interpreted to be dominated by avalanching processes, as fluvial tractive currents are less significant compared to facies F2a.

Mud drapes, reactivation surfaces, compound or sigmoid cross-bedding suggest that facies F2c and F2e record a tidal influence (Dalrymple & Rhodes, 1995). *Skolithos* indicate relatively high energy shallow-water environments so facies F2c and F2e are consistent with sediment reworking by tidal currents on the delta front (Figure 7J) (MacEachern *et al.*, 2005). Facies F2c is interpreted as resulting from the combination of deltaic avalanching and tidal tractive currents reworking in the middle part of the foresets. Whereas facies F2e and F2f are interpreted as tidal dunes or tidal bar deposits formed by tidal and subordinate currents preserved in between deltaic flood events and formed on the foresets. According to the 17% ratio from (Dalrymple & Rhodes, 1995), tidal dunes of 1m to 1,5m in thickness would have formed at a water depth comprised between 6 m to nearly 10 m.

In contrast to the preceding F2c facies, F2d does not exhibit evidence of tidal influence. Based on the more intense bioturbation, this facies is associated with the lower part of the foresets in the delta front, mainly dominated by avalanching processes.

### 3.1.3 FA 3: Deltaic mouth bar bottomsets

*Description* – Facies association FA 3 is present at various locations within the study area, particularly at the bottom of FA 2 clinoforms. FA3 consists of centimetre to decimetre-thick beds of very fine to medium-grained sandstone, organized in numerous fining-up cycles within thickening and coarsening-up sequences. Some coarser-grained deposits organized in sandbars were also recognized. Based on stacking patterns and dominant sedimentary structures, four facies are identified (1) Fine-grained sandstone with dunes or hydraulic jumps (F3a, Figure 8A), (2) very fine-grained sandstone with ripples

(F3b, Figure 8A, Figure 8D) Coarse-grained sandstone with sigmoidal cross-bedding (F3c) and (3) finely laminated silty claystone (F3d).

F3a and F3b deposits may contain mud clasts or mud drapes, organic matter debris, oxidized nodules, occasional nummulites, and rare annelid tubes (Figure 8C). F3c deposits are organized in pluridecimetre- to plurimetre-thick dunes with reactivation surfaces, and possible subordinate current ripples along foresets (Figure 8G). The dunes are dipping NNW (≃N310°), and they are interbedded with the finer and more argillaceous deposits of F3d, showing lenticular or wavy bedding, occasional current ripples with mud drapes (Figure 8F).

Facies F3a, F3b and F3d exhibit heavy bioturbation (BI up to 5, Figure 8B and Figure 8C), and typical trace fossil assemblages comprise common *Ophiomorpha* for all facies, *Thalassinoides* for facies F3b, F3c and F3d, *Skolithos* and *Zoophycos* for facies F3a, *Planolites* for Facies F3b and *Rosselia* for facies F3c.

*Interpretation* – Facies F3a and F3b are interpreted as bottomset deposits dominated by gravity flow on the low-gradient slope of the delta with sufficient hydrodynamic energy to record sedimentary structures. This interpretation is based on the high bioturbation index (BI up to 5) indicating a low sediment supply, the low angle bedding and the *Zoophycos* ichnofauna, indicating a more distal environment (Knaust, 2017)

Facies F3c and F3d are interpreted as tidal bars deposits because of the sigmoid cross-bedding, the reactivation surfaces and the clay couplets (F3d). This is consistent with the *Rosselia* trace fossils that are only found in facies F3c (Figure 8E) and that are a clue for high sedimentation rates and repeated erosion (Knaust, 2017). The different thicknesses of the tidal bundles highlight the neap-spring water cycles (Figure 8H).

The tidal bars observed in the bottomsets are larger than those identified on the foresets (facies F2e and F2f). Their thickness can reach 15 m and they are estimated to be kilometre-long and wide (1-2 km in width and up to 10 km in length (Leuven *et al.*, 2016; Michaud & Dalrymple, 2016). Based on the 1 m to 2,5 m thick dunes, the water depth could reach between 10 m and 15 m (Nio & Yang, 1991; Dalrymple & Rhodes, 1995; Martinius & Van den Berg, 2011).

### 3.1.4 FA 4: Low-energy mixed distal deposits

*Description* – Facies Association FA 4 is infrequently observed on outcrop but well-represented in cores. It occurs adjacent to facies association FA 3 and transitions to Facies Association FA 5. This facies association consist of bioturbated medium-grained (F4a) or fine-grained (F4b) sandstones, or nummulitic calcareous deposits (F4c).

Facies F4a and F4b are heavily bioturbated, lacking visible sedimentary structures (Figure 9A, Figure 9B), and frequently contain shell fragments, fine organic matter debris, and occasionally pyrite or mud clasts. They can be contorted (Figure 9D) or be affected by flame structures.

Facies F4c comprise wackestone to grainstone (or rudstone), dominantly composed of nummulites (with few alveolina, orbitolites, or miliolids) and locally with millimetre to pluricentimetre-sized bivalves, gastropods or corals fragments (Figure 9C).

The facies association exhibits a high degree of bioturbation, with the BI ranging from 2 to 5, and a diverse ichnofauna, including *Ophiomorpha*, *Planolites*, *Teichnichnus*, *Scolicia*, *Skolithos*, *Zoophycos* and *Palaeophycus*.

*Interpretation* – FA 4 deposits are associated with the transition between the distal part of the delta front and the inner part of the pro-delta. This is supported by intense bioturbation and *Teichichnus*, *Zoophycos*, *Scolicia* trace fossils indicating low- to moderate-energy conditions. The dominant processes are tidal currents or gravity flows, but bioclastic development conditions are permitted during low sediment supply periods. The local presence of hermatypic corals in facies association FA4 argues for an environment in the photic zone, with a water depth of probably less than 20 m (Olivier *et al.*, 2004).

#### 3.1.5 FA 5: Fine pro-delta deposits

*Description* – Facies Association FA 5 represents the distalmost deposits observed in both outcrops and cores and are predominantly found at the base of the sand body Y. This facies association is characterized by shaly grey marls enriched in foraminifera, primarily nummulites (Figure 9H). Depending on grain-size and dominant allochems, two facies are identified: (1) shaly to silty grey marls with numerous shell debris and (2) grey marls enriched in floating nummulites (F2b, Figure 9F and Figure 9G). Facies F5a shows abundant millimetre to centimetre-sized bivalve debris, gastropods, and echinoderms, sometimes concentrated in centimetre-thick accumulations (Figure 9E). Both facies' deposits can contain occasional pyrite and organic matter debris.

Bioturbation levels are moderate (BI between 0 and 3), represented mainly by *Palaeophycus* (Figure 9G).

*Interpretation* – FA5 deposits include hemipelagic marls and are dominated by decantation processes. This, plus the abundance of Nummulites indicate calm open marine environments, far from clastic input (Racey, 2001). The shell debris lags suggest sedimentation between the storm wave base and the fair-weather wave base in a storm-dominated environment of the pro-delta (Puga-Bernabéu & Aguirre, 2017).

### 3.1.6 Facies groups for interpretation

Ten facies groups were created in order to simplify the interpretations of the digital outcrop models. Facies were grouped (i) following facies associations or genetic processes (Table 2), (ii) because of their poor conditions on outcrops which did not allow their differentiation (for facies of FA3, FA4 and FA5) or (iii) to cluster tide-dominated faces (facies F2e, F2f, F3c, F3d). Facies F3a and F3b were grouped in the interpretation under their facies association name, "FA3 – Deltaic mouth bar bottomsets", because they are not easily distinguished on the DOM.

Facies of facies associations FA 4 and FA 5 were respectively grouped together because of their poor outcropping conditions.

| |
|---|
| F1a - Highly bioturbated silty to medium sandstone enriched in shells |
| F1b - Coarse sandstone with trough cross-bedding |
| F2a - Medium sandstone with trough cross-bedding |
| F2b - Medium sandstone with planar cross-bedding |
| F2c - Medium sandstone with cross- or compound-bedding |
| F2d - Massive structureless medium sandstone |
| Tidal dunes and bars |
| FA 3 - Deltaic mouth bar bottomsets |
| FA 4 - Low-energy mixed distal deposits |
| FA5 - Fine pro-delta deposits |

*Table 2 - Facies and facies associations used for interpretation.*

## 3.2 Depositional sequences

The cored section of well RODA 1 is used as a reference well to describe the interpreted vertical sequences as it crosses all the recognized delta mouth bars, except for the latest parasequence (Lobe 7, Figure 10). Prograding deltaic lobes are composed of conformal bedsets deposited during relative sea-level falls. They are stratigraphically bounded by an MFS at the base and an MRS at the top.

The Maximum Flooding surfaces (MFS) are better expressed at the top of each of the sandstone bodies comprising Y (Y1, Y2, Y3; (Joseph *et al.*, 1993)). These surfaces extend over kilometres, overlying deposits reworked by tidal currents and distal deposits deposited during the relative sea level rise. Four major MFS have been recognized, including the pluri-decimetre thick bioclastic beds at the base and the Plateau Limestone at the top levels. Those MFS segment the Y sandbody into three units corresponding to Y1, Y2 and Y3 from (Joseph *et al.*, 1993) where Y3 is equivalent to Y3 and Y4 from

(López-Blanco *et al.*, 2003) (Figure 10). Some of these sequences can be subdivided into higher-order (fifth or sixth-order cycles *sensu;* (Vail *et al.*, 1977)) and are formed through delta lobes amalgamation.

The Y1 sequence is composed of four delta lobes comprised respectively between the base surface and MRS 1 (Lobe 1), MFS and MRS 2 (Lobe 2), MFS 3 and MRS 3 (Lobe 3) and MFS 4 and MRS 4 (Lobe 4). Transgressive deposits lie at the top of the Y1 sequence, capped by MFS 5, which separates Y1 from Y2. The sequence Y2 is composed of the Lobe 5, between MFS 5 and MRS 5 and is overlaid by the deposits from the second major transgressive period (between MRS 5 and MFS 6). The last sequence Y3 is composed of two delta lobes 6 and 7 respectively between MFS 6 and MRS 6 and MFS 7 and MRS 7 (Lobe 7 is poorly recorded in well RODA 1 and is better developed laterally). Finally, the top part of the Y sandbody, comprised between MRS 7 and Top Y surfaces recorded sediments from the beginning of the flooding of the system up to the Plateau Limestones.

## 3.3 Outcrop interpretation

The identified stratigraphic surfaces as well as the ten grouped facies and facies associations (Table 2) have been coded along the seven digitized wells, the nineteen vertical sections, and mapped along the entire outcropping cliffs of the DOM (see Figure 11, Figure 12, Figure 13). The Facies 3D mapping on the outcrops highlighted a few elements:

The interval deposited during the transgressive period capped by the MFS 5 is better developed and thicker in the Roadcut outcrop than in the El Villar outcrop located eastwards (Figure 11, Figure 12). In this transgressive setting, pluri-decimetre thick tidal dunes formed above Lobe 4 (Figure 12). Also, larger tidal bedforms could develop during transgressive periods, as shown at the base of the Roadcut outcrop in the interval between MRS 2 and MFS 3, where a plurimetre-thick tidal bar shows sigmoidal bedding dipping N300° (Figure 11).

During delta lobes progradation phases, metre-thick tidal dunes formed on top of Lobe 2 formed by dominant currents (ca. N320° Figure 12). Larger tidal bars also developed in the delta lobes clinoforms, mostly along the foresets: For example, on the Roadcut outcrop (Figure 11), a plurimetre-thick tidal bar was found north-west to the vertical section Roadcut in Lobe 4. It lied on foresets facies deposits (F2c) and according to the paleocurrents directed to the south (N190° on average on the corresponding rose diagram, Figure 11), it was formed by the subordinate flood currents.

Moreover, the Las Forcas outcrop, which is centred on the Lobe 5, features a tidal bar covered by the deposits of the following fluvial flood supply influxes (Figure 13). This tidal bar shows locally bidirectional cross-bedding formed by both dominant and subordinate currents.

213 The plurimetre-thick clinoforms of the deltaic lobes are well visible on the Roadcut outcrop, especially
214 in the lobes 4 and 5 (Figure 11). While lobes 5 and 6 show clinoforms dipping westwards (N255°) to
215 southwards (N190°) respectively, lobe 4 seems to prograde north-westwards (N290°). Furthermore,
216 within a single lobe, the direction of progradation can vary depending on location. For example, in lobe
217 5, the clinoforms at the Las Forcas outcrop dip further to the north-west than at the Roadcut outcrop
218 (N295°), suggesting a stronger tidal influence (Figure 11, Figure 13).

219

## 220 3.4 Stratigraphic surfaces correlations, facies architectures and delta lobes
## 221 reconstruction

222 Figure 14 shows the correlations of vertical sections based on the sequential division presented above
223 (section 3.2 Depositional sequences) and the interpreted outcrops (section 3.3 Outcrop interpretation)
224 along the delta progradation axis (NE to SW) for cross-section 1 (Figure 14) and on strike for cross-
225 section 2 (Supplementary Data, Figure 22). If MRS are well correlated laterally, MFS may be subject to
226 erosion by overlying sequence boundaries. For example, MFS 5 and MFS 6 can be correlated in the
227 southwestern part of the study area (RODA 5 to RODA 1 sections on cross-section 1; Figure 14) but
228 were eroded by the overlying deposits.

229 The parasequences deposits are genetically linked, meaning that within one lobe, all facies were
230 deposited in lateral continuity. Deposits transition vertically from bottomset facies (FA4) at the bottom
231 of the delta lobes to foresets and topset facies (e.g., Lobe 1 in Figure 14). Lateral facies transitions also
232 illustrate the delta lobes progradation from the most proximal part (e.g., in Codoneras and Serraduy
233 South sections) to the most distal area (e.g., RODA 4 and RODA 5). In between the delta lobes, the
234 distal transgressive deposits and reworked sediments composing tidal bars are especially developed in
235 between MRS 4 and MFS 5 (Figure 14) and in between MRS 5 and MFS 6 (Supplementary Data, Figure
236 22). These more silty interlobe deposits segment the sandstone bodies on the scale of the Y sandbody
237 and could therefore play the role of reservoir heterogeneities.

238 Figure 15 illustrates details of such lateral facies variations on a 2D cross-section of Lobe 5 from a
239 proximal pole (Zipaguerne 1) in the north-eastern part of the study area to a distal pole (RODA 7) in
240 the southern part of the study area. In the vertical section Zipaguerne 1, the bedsets of show a
241 coarsening-up trend, trough cross-bedding and some early-diagenetic calcite-cemented nodules. This
242 entire portion of section is interpreted as facies F2a deposits. These deposits transition laterally to a
243 vertical section (Roda 1) with finer deposits at the base of the interval (38.5 to 39.5 m depth), highly
244 bioturbated with numerous shell clasts and a few benthic foraminifera (mostly nummulites). These
245 deposits are interpreted as bottomset deposits (FA4) and are overlain by coarser grained deposits with

cross and compound bedding. The vertical grain size trend is still coarsening-up and there can be simple or compound dunes (forming tidal bars) intercalated in between the bedsets interpreted as facies F2c. Finally in the more distal part of the lobe (Roda 7 section), the vertical succession shows even more variability in terms of facies: the deposits are fine grained, with intense bioturbation and very few sedimentary structures visible at the base (FA5; between 50 and 53 m depth). These deposits transition vertically to deposits structured in pluri-decimetre-thick coarsening-up sequences with current ripples, that are interpreted as bottomsets deposits (FA3). They are overlain by even coarser grained deposits, still in pluri-decimetre-thick coarsening-up sequences with compound, planar or trough cross-bedding that are interpreted as delta mouth bar foreset deposits, respectively F2c, F2b and F2a. This vertical facies succession illustrates therefore the delta lobe progradation that is also visible laterally on the present 2D cross-section between the three vertical sections.

The 3D mapping facies point cloud is shown in the background of Figure 16 (and in Supplementary Data Figure 25, Figure 26) and was used to draw the different facies belts: For each lobe (i.e., each interval between MFS and MRS), the predominant facies in terms of thickness (or the most proximal in case of similar proportions) were used to trace the limits of facies. The proposed extents of the delta lobes in Figure 16 were defined based on the location of the most distal facies in each interval and on paleocurrents measurements corrected from the regional dip (dipping 8° towards N170 after measurements). The paleocurrent measurements come from various sources (field measurements, DOM measurements, well data from dipmeter) and were acquired either on the inclined bedsets that are part of the delta lobe clinoforms or on the tidal dunes (simple or compound, part of tidal bars) foresets (Figure 16). When no data was available to constraint the delta lobe extents in width for example, length and width ratios from (Reynolds, 1999) were used.

Facies quantification

The facies 3D interpretation enabled the extraction of quantitative data from the DOM interpretations, such as facies proportions or depositional system dimensions. Figure 17 illustrates the outcropping facies proportions depending on the location in the deltaic system. The most proximal deposits (F2a and F2b) are predominant in the northeastern part of the study area, with their proportions diminishing westward and southwards, shrinking from 64 % to 16 %. Facies from facies association FA 1 were observed either in cores (F1a) or very locally in the DOM (F1b observed in Serraduy South and Codoñeras vertical sections, see Fig. 1B for location), and thus their proportion is not high enough to appear on the charts.

Tidal influence or dominance, recorded by facies F2c, F2d, F2e, F3c and F3d, is more pronounced in the more distal part of the Y sand body. This region's average proportion of tidal sand bodies (tidal dunes and bars) reaches ca. 10 %.

Figure 17 enables to estimate the predominant sedimentary process in the different zones of the outcrops: it is possible to estimate the predominant sedimentary process according to the different sedimentary structures in the different facies. As facies F2c (Medium sandstone with compound-bedding) and the interpreted tidal dunes and bars are considered to be generated by tidal currents, the percentage of tidal-generated structures is comprised between 19 % and 51 %, depending on the zone (Figure 17). Overall, the percentage of tidal-dominated or tide-influenced facies is 37 %, the rest being fluvial-dominated.

# 4 Discussion

This study supplements previous studies on ancient mixed deltaic systems by delivering the first high-resolution and multiscale DOM interpreted in both geometries and facies of a mixed ancient delta. Based on the sedimentary structures, the facies and facies association proportions (See part 3.4 in Results) and paleocurrent measurements, the Roda Y sand body is interpreted as a fluvial-dominated and tide-influenced delta, consistent with earlier studies (Crumeyrolle *et al.*, 1993; López-Blanco *et al.*, 2003; Tinterri, 2007; Leren *et al.*, 2010; Michaud, 2011; Martinius, 2012). However, the cross-sections (Figure 14 & Supplementary Data, Figure 22), and the interpreted high-resolution and multiscale DOM have led to a better-constrained and detailed architecture of the Y sandbody. These outcomes further allow for a refined interpretation of the sedimentary bodies generated by tidal currents within this mixed deltaic system.

## 4.1 Variability of mouth bars architecture and quantification of their characteristics

In Figure 16, the river paleo-flows indicate a general trend comprised toward the southwest and the west (between N210° and N310°), but some lobes appear to deviate towards the tidal direction, such as lobes 1, 2, 4 and 7. These paleocurrent directions have already been documented in the literature (Joseph et al., 1993; Leren et al., 2010) but have never been commented on yet. This kind of variability could result from the feeding alluvial pathway variations or from the interaction between river flows and tidal currents. This could indicate a shift in the dominant process regime described by (Longhitano & Steel, 2017); (Longhitano & Nemec, 2005; Uroza, 2008)) with regard to its position in the stratigraphy. For example, Lobe 4 is the uppermost lobe in unit Y1 before the major transgressive period comprised between MRS 4 and MFS 5. Lobes 5 and 6 are part of respectively units Y2 and Y3, and lobe 7 is the uppermost lobe of the Y sandbody, slightly backstepping, before the transgression period in which the Plateau Limestone was deposited. Lobe 7 then shows a “tidally dominated deflected delta front” that coincides with the progradation maximum of the Y sandbody before the transgression phase that separates it from the Z sandbody.

Figure 16 displays considerable variability in the deltaic lobes' size and their direction of progradation, suggesting potential source variability or an increasing tidal reworking. The interpreted dimensions of the deltaic lobes are shown in the table below and the ratios between the lengths, widths and thicknesses are plotted in comparison with other deltaic lobes datasets (Figure 18). The average lobe length is 4,3 km, the average width is 2,6 km, the average thickness is 20 m, and the dimensions of the delta lobes increase upwards as they prograde further basinward.

Our interpreted lobe dimensions are smaller than those in the literature (Reynolds, 1999): the lobe's lengths range from 2,6 km to 7,1 km while they reach 10 km long in Reynolds (1999). A reason could be that Reynolds (1999) study considers data from the Book Cliffs formations, that were deposited I a different geological context than the Roda Sandstone. The Roda Sandstone formed in a much narrower foreland basin than the Westen Interior Seaway, and even considering the south-Pyrenean basin settings, the Roda Sandstone is considered a small delta system compared to the Sobrarbe delta system deposited in a very comparable geological context (Grasseau *et al.*, 2019).

On another hand, our interpreted lobes dimensions are larger in comparison to those of the archive data (Joseph *et al.*, 1993; Joseph, 1994). It can be explained by the fact that the sandbody Y subunits Y2 and Y3, corresponding respectively to lobes 5 and 6 were decomposed in more sub-units than in the present study. However, in this study, we found no evidence to support this. Finally, the cross plots show that the presented lobes' dimensions fit in realistic ranges, with similar ratios to those from Joseph *et al.* (1993) and Joseph (1994).

DOMs helped at better understanding of the internal architecture of the delta system (Eide *et al.*, 2016; Rubi *et al.*, 2018; Howell *et al.*, 2021; Atlas *et al.*, 2023). First, the georeferenced field and well data enable improved correlations, especially between areas that are difficult to correlate, such as the two sides of the Isabena river, or between the wells and the outcrops. Furthermore, multiplying dip measurements which can be time-consuming in the field or that cannot be carried out *in situ* (Hodgetts, 2013; Marques *et al.*, 2020) helped to determine the different lobe directions of progradation (see sections 3.3 and 4.1). Finally, other measurement tools enabled to extract quantitative data about the geometries of the interpreted lobes, to be compared to literature data.

## 4.2 Water depth estimation of clinoforms using DOM restoration

3D mapping of facies in a finely resolved georeferenced system can also be used to estimate water depths from differences in elevation corrected for structural dip. The 3D facies point cloud was

displayed in a 3D visualisation software (Petrel®), allowing 3D distance measurements, and the following procedure was applied:

First, for lobes 3, 5 and 6, distance measurements were taken between different facies points in different locations of the study area and one reference point on the DOM which is the most proximal point of the facies point cloud for this given interval (hereafter called the "proximal reference point"). Coordinate and elevation deviations ΔX, ΔY and ΔZ were collected and used to correct the measured elevation difference ($\Delta Z_{mes}$) from the structural dip (5,5° toward N170°) using a trigonometric calculation (Figure 27). For simplification purposes, the calculation assumed that the structural dip was southward (N180°).

$$\Delta Z_{corr} = \Delta Z_{mes} - (\tan(5{,}5°) \times \Delta Y_{mes})$$

This corrected elevation difference ($\Delta Z_{corr}$) was then used to calculate paleo-bathymetries based on the estimation of the water depth of the proximal reference point. For the 3 lobes (Lobe 3, Lobe 5, and Lobe 6), the proximal reference point was placed in facies F2a which is interpreted as intertidal deposits based on the presence of *Macaronichnus* (MacEachern *et al.*, 2005), the medium to coarse grain-size and the high hydrodynamic currents to form trough cross-bedding. The considered water depth for the proximal reference point is 0 m, knowing that the tidal range was estimated to be 3,6 m (Martinius & Van den Berg, 2011) (see section 3.1.1). The resulting water depth estimations for each facies are shown on the box plot graph of Figure 19. Some points show positive paleo bathymetry estimates, i.e., above the mean sea, and they may correspond to high tide deposits, although no evidence of tidal recording was found in this part of the delta. The water depths of the tide-generated structures (tidal dunes and tidal bars) were estimated by another method: based on the rule of thumb linking the height of tidal dunes to with water depths (Dalrymple & Rhodes, 1995).

These values can be underestimated because some dunes that are part of tidal bars were truncated. If we consider that the maximal thickness of the dunes forming the tidal bar reached 2 to 3 m, the water depth would be comprised between 12 and 18 m.

Even though this method is quite simplistic and includes numerous sources of incertitude (e.g., structural dip corrections, water depth of the proximal reference point), it allows to obtain relative water depth estimations of the facies compared to the proximal reference points and thus assess the slope of the delta lobes. Figure 19 illustrates the facies distribution on a delta front slope: facies of the facies association FA2 ("Deltaic mouth bar foresets") show the widest distribution of values, and the median values comprised between -10 m (for F2a) and -25 m (F2b). Facies in the FA3 association ("Deltaic mouth bar bottomsets") show the same distribution as facies F2b and F2c in terms of range and median values, ca. 20 m. Finally, the paleo bathymetry values for facies in the FA4 association show

a real deepening, with medians between around -35 m and -40 m. The maximal water depth values are consistent with water depth estimations of the basin based on palaeo-fauna studies and that are comprised between 30 m and 80 m (Martinius, 1995; Molenaar & Martinius, 1996; Torricelli *et al.*, 2006). These values are consistent with various modern tide-dominated or tide-influenced deltas such as the Yangtze River delta (Hori *et al.*, 2002) and the Fly River delta (Harris *et al.*, 1993).

## 4.3 Tidal expression in the fluvial-dominated deltaic record

The current study proposes two depositional models for regressive and transgressive settings that integrate tidal reworking (Figure 20) and key diagnostic features better to identify the different process-generated sandbodies (Figure 21). These features could be applicable to other ancient mixed deltaic systems with tidal reworking processes. The multiplication of paleocurrent measurements and the multiscale characteristic of DOMs facilitated the deciphering of intermixed fluvial-dominated and tide-reworking currents. Thanks to the coverage and the high resolution of the DOM, it can be interpreted from the scale of the deltaic system (ca. 10 km x 5 km) or a portion of the system (e.g., this study), to a detailed work on one sandbody that shows a more complex internal structure caused by the tide-reworking (e.g., Las Forcas, Figure 13). This feature helped to recognize the different tide-generated structures (tidal dunes, tidal bars, compound-bedding) on the outcrop and identify their position stratigraphically and spatially in the delta.

Depending on the position in the stratigraphic sequences or in the lobe, different tide-generated or tide-influenced sandbodies can be formed with various preservation degrees.

### 4.3.1 Regressive settings

During regressive settings (Figure 20A), deposits in the uppermost part, at the top of the delta lobe (topsets), are dominated by river flood flow processes with no evidence of tidal reworking influence. The corresponding facies are mostly classified in the facies association FA 1 (“Deltaic mouth bar topsets”) or in the facies association FA 2 (“Deltaic mouth bar foresets”): F2a (Medium sandstone with trough bedding) and F2b (Medium sandstone with planar cross-bedding). These facies constitute the topsets and foresets of the delta lobes clinoforms with a water depth ranging between 0 and 25 m (Figure 19).

On the delta front, some deposits can record tidal influence during the lobe progradation phase, with various degrees of preservation depending on the fluvial input (Figure 21).

When the fluvial input is high, mixed fluvial and tidal sedimentary structures can be found widely on the delta front, attesting to the constant tidal reworking during the lobe progradation phases: flood-derived sediment pulses are t immediately reworked by tidal currents to form foresets with compound

409 bedding, corresponding to facies F2c (medium sandstone with cross-or compound bedding). The angle
410 of the cross-stratification can appear quite low, but when the tidal currents are perpendicular to the
411 progradation direction of the lobe, the bedding may even appear inverted compared to the set's
412 inclination (Figure 20A). These reworked deposits correspond to the “compound bars” as defined by
413 (Crumeyrolle *et al.*, 1993) and partly to the “Delta front deposits” facies association of (Leren *et al.*,
414 2010).

415 Metre-thick simple dunes are formed by tidal current reworking when the fluvial sediment supply
416 ceases or diminishes. These dunes can be found on top of the bedsets surfaces, which form the
417 clinoform foresets, and more frequently towards the top of the lobe (Figure 15, Figure 20A, Figure 21).
418 Their predominance towards the top of the lobes can either be explained by more intense reworking
419 by tidal currents when the lobe was abandoned or these tidal dunes were preserved during periods of
420 less frequent flooding events that could erode them. These tidal deposits may then otherwise be poorly
421 preserved elsewhere in the lobes.

422 During longer periods of fluvial activity decrease, these tidal dunes can stack and form compound tidal
423 bars (Dalrymple & Rhodes, 1995) (Figure 7, Figure 20A, Figure 21). Those plurimetre-thick sand bodies
424 lie on the delta front slope and show sigmoidal cross-bedding with bundles recording mostly the
425 dominant current (~N320° ; (Nio & Yang, 1991; Michaud & Dalrymple, 2016) sometimes only the
426 subordinate current (~N140°), and locally both dominant and subordinate currents (Figure 7, Figure
427 20A). The presence of reactivation surfaces within tidal bars and the higher bioturbation intensity
428 support the tidal bar interpretation (See Facies F2d and Facies F2e in section 3.1.2) (Allen &
429 Homewood, 1984; MacEachern *et al.*, 2005; Shchepetkina *et al.*, 2019). They testify for a higher
430 preservation degree of the tidal reworking, and/or a more significant influence of tidal reworking.

431 4.3.2 Transgressive settings

432 During relative sea-level rise, the sediment supply cannot compensate for the relative sea-level rise,
433 and the system retrogrades. The fluvial input was not well recorded during this period, and the tidal
434 currents were the dominant processes involved in the sedimentary record. As a consequence, the
435 sediments deposited during the regression are prone to be reworked by the tidal currents and thus
436 shape stacked dunes migrating in the direction of the dominant tidal current (e.g., ebb currents in this
437 case) that finally form tidal bars preserved on top of the toe of regressive foresets and bottomsets,
438 where the subtidal current velocity is the highest (Figure 20B). Hence, the tidal-generated structures
439 are larger and can form in deeper settings: tidal bars lie on the bottomsets, at estimated water depth
440 of 10 m to 20 m (see section 3.1.3; Figure 20B). Sigmoidal cross-stratifications, mud couplets,
441 reactivation surfaces and *Rosselia* ichnofossil can be found in these tidal structures. Moreover, the

neap-spring cycles are generally better expressed in the bundles' thicknesses, and there is often an angle (20° up to 50°) between the direction of progradation of the tidal bar and the tidal dominant current direction, measured in the DOM in the area of Point of interest 3 (Figure 4). This testifies for lateral accretion (Dalrymple & Rhodes, 1995; Olariu *et al.*, 2012a). These remarkable structures correspond to the "sand ridges" as described by Michaud (2011) and were formerly interpreted as tidal bars (Nio & Yang, 1991; Crumeyrolle *et al.*, 1993; Leren *et al.*, 2010; Martinius, 2012).

## 4.4 Controlling factors of tidal recording in mixed fluvial-tidal deltas

Paleomorphology of the basin might have significantly impacted the amplification of tidal currents in the Roda area. During the Ypresian, the Graus-Tremp-Ager basin was opened towards the northwest, and several sub-basins were originated by local highs originated by the Montsec blind thrust (Eichenseer, 1988; Castelltort *et al.*, 2017; Chanvry *et al.*, 2018; Vaucher *et al.*, 2024) (Figure 1), and forming a ridge separating several depocenters.

This elongated basin could have funnelled tidal currents because of the converging masses of water (Pugh, 1987; Pratt, 1990). As a result, the tidal currents' velocities could increase with a "tunnelling effect" due to the shape of the basin, with currents flowing parallel to the coastline and in competition with the fluvial currents in the vicinity of deltaic systems. According to the basin geometry, we could deduce that the dominant tidal current (~N320°) corresponds to the ebb current and the subordinate current (~N140°) to the flood currents.

A similar pattern occurred in the Aren Sandstones, where demonstrated tidal influence was observed at the beginning of the Aren Sandstone delta progradation (Nagtegaal *et al.*, 1983), at the beginning of flexuration induced by the Boixóls thrust fault activity that started to create sub-basins. As progradation advanced basinward, the amplification of tidal currents diminished, and their impact on deposits lessened in favour of wave action. Similarly, the silico-clastic systems of the Montanyana Group that deposited after the Roda Sandstone and that have prograded further in the Graus-Temp Basin show increasing wave influence (especially the Perarrua Sandstone, part of the Upper Montanyana Group) (Nijman, 1998).

Moreover, López-Blanco *et al.* (2003) suggest that the tidal currents could have been funnelled and increased along a growing gentle folds system, influencing facies deposition, current patterns, and sediment dispersal. The influence, however, should remain limited, as no syntectonic unconformities are observed in the formation, and sedimentation rates consistently exceeded fold growth rates (López-Blanco *et al.*, 2003).

If the tidal reworking is constant, the preservation degree of the tidal expression depends on different factors:

In a regressive setting, the tidal currents are recorded in the sediments with different characteristics that depend on the fluvial activity. The compound bedding is preserved on the delta front even during periods of progradation of the deltaic lobe fed by high sediment supply. The tidal dunes and tidal bars intercalated in the foresets deposits are deposited and preserved between flood-derived foresets construction or during the lobe abandonment. The lobes making up the Y1, Y2, and Y3 sub-units are thought to record autocyclic factors as switching or abandonment lobes because the distal deposits overlying them are less continuous over large distances as they may be for the major transgressive intervals separating the Y1 to Y3 sub-units.

The development and preservation of larger tidal bars on bottomsets are permitted by the weakness of the fluvial currents compared to the tidal ones observed during transgressive periods of fourth-order cycles. This periodicity could potentially be attributed to climatic variations. Because the Lower Eocene lacks evidence for widespread continental ice sheets and features hyperthermal events (e.g. The Early Eocene Climate Optimum from 53.56 to 49.14 Ma; (Zachos *et al.*, 2001; Westerhold *et al.*, 2020)) (Figure 2), glacio-eustatic variations seem unlikely. However, similar climatic variations impacting sedimentary inputs, as recently demonstrated in the Castigaleu Formation (52.2–50.6 Ma), could act as controlling factors on the fourth-order cyclicity. A study by Vaucher *et al.* (2024) integrating carbon and oxygen stable isotope profiles correlated with magnetostratigraphic curves suggests that the deltaic progradation of the Castigaleu Formation (52.2–50.6 Ma) may be associated with heightened sediment transport and continental weathering resulting from intensified hydrological conditions during hyperthermal events. This underscores the influence of climate on stratigraphic records, which can be underestimated in active foreland basins. Similar climatic variations could have impacted the stratigraphic architecture of older shallow-marine systems in the Roda Sandstone Formation (Figure 21).

# 5 Conclusion

The Y sand-body of the Roda Sandstone (Ypresian, lower Eocene in southern Pyrenees) exhibits a complex internal architecture and facies assemblage caused by tidal-reworking of fluvial deltaic deposits. Our dataset integrated classical sedimentology fieldwork along with near-outcrop cores description and the acquisition of this formation's largest georeferenced digital outcrop model (DOM) to date.

Ten facies or facies associations were defined, and the DOM interpretation combined with two stratigraphic cross-sections enabled the identification of seven delta lobes, whose directions of

progradation vary from southwest to northwest. They gradually shift to a tidally dominated-deflected delta front as the delta progrades. The objectives of this work were to attempt to clarify the tidal reworking process by defining key sedimentary features generated by tidal currents and propose a depositional model for mixed fluvial-dominated and tide-influenced ancient deltas.

- Most proximal deposits, particularly in the upper part of the foresets and in the topsets of the delta front system, don't record any tidal influence.
- Foresets and bottomsets are, on the contrary, largely affected by tidal currents. Specific facies identified in this study are characterized by the competition between fluvial and tidal processes, such as compound bedding, predominantly observed within the delta foresets. Moreover, certain features like tidal dunes or bars are solely formed by tidal currents, with the former occurring during delta progradation phases and the latter during transgressive periods.

The fluvial input controls tidal structures within foresets: Tidal dunes are preserved when fluvial activity decreases or ceases, forming dunes or bars intercalated between foresets. The lower supply of river sediment during transgressive periods of fourth-order cycles, influenced by climatic variations, allows for the preservation of larger tidal bars on bottomsets.

This detailed work on the geometries and facies distribution within the Roda deltaic system was made possible thanks to the availability of detailed Digital Outcrop Models (DOM), which give a lot of well-documented advantages) — such as data collection from inaccessible areas, viewpoint manipulation, enhanced fieldwork time management, and training applications. This study highlights several contributions of DOMs in complementing traditional sedimentological methods. This research expands the utility of DOMs in three key aspects:

- First, DOMs offer an improved understanding of the internal architecture of deltaic systems. Integrating georeferenced field and well data enhances correlation, particularly in challenging areas like opposite sides of the Isabena River, or between wells and outcrops. The ability to perform numerous dip measurements, which are often labour-intensive or infeasible in the field, facilitates the determination of progradation directions for different lobes. Additionally, DOMs allow for the extraction of quantitative data on lobe geometries, aiding comparisons with existing literature.
- Second, DOMs assist in distinguishing between fluvial-dominated and tide-reworked currents by multiplying paleocurrent measurements directly on the digital model and the multiscale analysis they enable. The extensive and high-resolution coverage of DOMs permits interpretation at both system-wide and detailed sandbody levels, revealing complex internal structures and enabling the measurement of tidal features to estimate paleo-water depths.

- Finally, DOM-based facies mapping provides comprehensive qualitative and quantitative insights into facies distribution within lobes and along proximal-distal gradients, offering a more detailed understanding and representation of sedimentary heterogeneities than classical methods. This quantitative data further refines paleoenvironmental interpretations, including water depth estimations.

## 6 Authors contribution

Perrine Mas - Conceptualization, Data Curation, Investigation, Methodology, Software, Visualization, Writing – Original Draft Preparation, Writing – Review & Editing

Raphaël Bourillot - Conceptualization, Investigation, Methodology, Project Administration, Supervision, Writing – Original Draft Preparation, Writing – Review & Editing

Rémy Deschamps - Conceptualization, Investigation, Methodology, Supervision, Writing – Review & Editing

Benjamin Brigaud - Conceptualization, Funding Acquisition, Investigation, Methodology, Project Administration, Supervision, Writing – Original Draft Preparation, Writing – Review & Editing

Bertrand Saint-Bezar - Investigation, Methodology, Software

Phillipe Razin - Investigation, Resources, Visualization

Eric Portier – Investigation, Resources

Adrien Henry - Data Curation, Investigation, Resources

Baptiste Hersant - Data Curation, Investigation, Resources

## 7 Acknowledgment

This work is supported by the UPGEO "UPscaling and heat simulations for improving the efficiency of deep GEOthermal energy" programme funded by the Agence Nationale de la Recherche [ANR-19-CE05-0032-01]. We are grateful to TotalEnergies for allowing us access to the cores and the archive data. We thank VRGS® and David Hodgetts for the academic licence and valuable support. We also thank Pix4D for the Pix4Dmapper academic licence. University Paris-Saclay benefits from the Schlumberger Software Donation Program, and we are grateful to Schlumberger for the academic licence for Petrel software. We sincerely thank Hugues Féniès for his assistance and discussions during the fieldwork.

## 8 Data Availability

Dataset of the 3D model containing the Digital Outcrop Model (DOM), field and interpreted data (logs, polylines, dips, 3D facies maps…) can be found at https://doi.org/10.57745/Y2OXPZ in the multidisciplinary repository Recherche Data Gouv, under the Creative Commons Attribution (CC BY 4.0) licence. The Digital Outcrop Model can be viewed in various 3D visualization, specialized interpretation, or geomodeling software (ArcGIS, Surfer, VRGS®, Petrel, Windows 3D Viewer, Apple 3D Model Viewer, etc.). The interpreted data can be imported into GIS or geomodeling software for visualization or

processing. The high-resolution interpreted Digital Outcrop Model can also be used for further studies or educational purposes.

# 9 References


**Agnini, C.**, **Monechi, S.** and **Raffi, I.** (2017) Calcareous nannofossil biostratigraphy: historical background and application in Cenozoic chronostratigraphy. *Lethaia*, **50**, 447–463.

**Ainsworth, R.B.**, **Vakarelov, B.K.** and **Nanson, R.A.** (2011) Dynamic spatial and temporal prediction of changes in depositional processes on clastic shorelines: Toward improved subsurface uncertainty reduction and management. *AAPG Bull.*, **95**, 267–297.

**Aliyuda, K.**, **Charlaftis, D.**, **Priddy, C.** and **Howell, J.A.** (2024) Analysis of facies proportions as a tool to quantify reservoir heterogeneity. *Mar. Pet. Geol.*, **170**, 107093.

**Allen, G.**, **Laurier, D.** and **Thouvenin, J.** (1979) Etude Sédimentologique du Delta de la Mahakam.

**Allen, J.R.L.** (1980) Sand waves: A model of origin and internal structure. *Sediment. Geol.*, **26**, 281–328.

**Allen, P.A.** and **Homewood, P.** (1984) Evolution and mechanics of a Miocene tidal sandwave. *Sedimentology*, **31**, 63–81.

**Atlas, C.E.**, **Morris, E.A.**, **Johnson, C.L.** and **Wroblewski, A.F.-J.** (2023) New approaches to the architectural analysis of deltaic outcrops: Implications for subsurface reservoir characterization and paleoenvironmental reconstruction. Sedimentologika. doi: 10.57035/journals/sdk.2023.e11.1051

**Backman, J.**, **Raffi, I.**, **Rio, D.**, **Fornaciari, E.** and **Pälike, H.** (2012) Biozonation and biochronology of Miocene through Pleistocene calcareous nannofossils from low and middle latitudes. *Newsl. Stratigr.*, **45**, 221–244.

**Barrel, J.** (1912) Criteria for the recognition of ancient delta deposits. *GSA Bull.*, **23**, 377–446.

**Bentham, P.** and **Burbank, D.W.** (1996) Chronology of Eocene foreland basin evolution along the western oblique margin of the South–Central Pyrenees. In: *Tertiary Basins of Spain*, 1st edn. (Ed. P.F. Friend and C.J. Dabrio), *Cambridge University Press*, 144–152.

**Berggren, W.A.**, **Kent, D.V.**, **Swisher, C.C., III** and **Aubry, M.-P.** (1995) A Revised Cenozoic Geochronology and Chronostratigraphy. In: *Geochronology, Time Scales and Global Stratigraphic Correlation* (Ed. W.A. Berggren, D.V. Kent, M.-P. Aubry, and J. Hardenbol), *SEPM Society for Sedimentary Geology*, 54, 0.

**Bhattacharya, J.P.** (1978) Deltas. *SEPM Spec. Publ.*, 237–292.

**Busch, D.A.** (1971) Genetic Units in Delta Prospecting. AAPG Bull. doi: 10.1306/819A3CCA-16C5-11D7-8645000102C1865D

**Cabello, P.**, **Dominguez-Lopez, D.**, **Murillo-López, M.**, **López-Blanco, M.**, **Garcia-Sellés, D.**, **Cuevas, J.**, **Marzo, M.** and **Arbués, P.** (2018) From conventional outcrop datasets and digital outcrop models to flow simulation in the Pont de Montanyana point-bar deposits (Ypresian, Southern Pyrenees). Mar Pet Geol. doi: 10.1016/j.marpetgeo.2018.03.040

**Castelltort, S.**, **Honegger, L.**, **Adatte, T.**, **Clark, J.D.**, **Puigdefàbregas, C.**, **Spangenberg, J.E.**, **Dykstra, M.L.** and **Fildani, A.** (2017) Detecting eustatic and tectonic signals with carbon isotopes in deep-marine strata, Eocene Ainsa Basin, Spanish Pyrenees. *Geology*, **45**, 707–710.

**Catuneanu, O.**, **Abreu, V.**, **Bhattacharya, J.P.**, **Blum, M.D.**, **Dalrymple, R.W.**, **Eriksson, P.G.**, **Fielding, C.R.**, **Fisher, W.L.**, **Galloway, W.E.**, **Gibling, M.R.**, **Giles, K.A.**, **Holbrook, J.M.**, **Jordan, R.**, **Kendall, C.G.St.C.**, **Macurda, B.**, **Martinsen, O.J.**, **Miall, A.D.**, **Neal, J.E.**, **Nummedal, D.**, **Pomar, L.**, **Posamentier, H.W.**, **Pratt, B.R.**, **Sarg, J.F.**, **Shanley, K.W.**, **Steel, R.J.**, **Strasser, A.**, **Tucker, M.E.** and **Winker, C.** (2009) Towards the standardization of sequence stratigraphy. *Earth-Sci. Rev.*, **92**, 1–33.

**Catuneanu, O.**, **Galloway, W.E.**, **Kendall, C.G.S. t C.**, **Miall, A.D.**, **Posamentier, H.W.**, **Strasser, A.** and **Tucker, M.E.** (2011) Sequence Stratigraphy: Methodology and Nomenclature. *Newsl. Stratigr.*, 173–245.

**Chanvry, E.** (2016) Caractérisation et facteurs de contrôle des distributions minéralogiques du Bassin Piggyback de Graus-Tremp-Ainsa (Espagne), à l'Eocène Inférieur. Phdthesis, Université de Lyon

**Chanvry, E.**, **Deschamps, R.**, **Joseph, P.**, **Puigdefàbregas, C.**, **Poyatos-Moré, M.**, **Serra-Kiel, J.**, **Garcia, D.** and **Teinturier, S.** (2018) The influence of intrabasinal tectonics in the stratigraphic evolution of piggyback basin fills: Towards a model from the Tremp-Graus-Ainsa Basin (South-Pyrenean Zone, Spain). *Sediment. Geol.*, **377**, 34–62.

**Coleman, J.M.** and **Wright, L.D.** (1975) Modern River Deltas: Variability of Processes and Sand Bodies. 99–149.

**Coll, M.**, **López-Blanco, M.**, **Queralt, P.**, **Ledo, J.** and **Marcuello, A.** (2013) Architectural characterization of a delta-front reservoir analogue combining Ground Penetrating Radar and Electrical Resistivity Tomography: Roda Sandstone (Lower Eocene, Graus-Tremp basin, Spain). *Geol. Acta*, **11**, 27.

**Crumeyrolle, Ph.** (2003) Stratal architecture and facies assemblages of the Roda Sandstone lowstand wedge (south-central Pyrenees). In: *AAPG International Conference and Exhibition*, 21–24.

**Crumeyrolle, Ph.**, **Claude, D.**, **Lesueur, J.L.** and **Joseph, Ph.** (1993) The Roda Deltaic Complex (Spain): Reservoir Stratigraphy of a Low Stand Prograding Wedge. AAPG Bull. doi: 10.1306/D9CB6B05-1715-11D7-8645000102C1865D

**Crumeyrolle, Ph.**, **Lesueur, J.L.**, **Claude, D.** and **Joseph, Ph.** (1992) Architecture et facies d'un prisme deltaïque de bas niveau marin: Les Grès de Roda (Bassin Eocène sud-pyrénéen) - Livret-guide de l'excursion A.S.F du 25 au 27 Septembre 1992.

**Dalrymple, R.W.** and **Rhodes, R.N.** (1995) Chapter 13 Estuarine Dunes and Bars. In: *Developments in Sedimentology* (Ed. G.M.E. Perillo), *Elsevier*, 53, 359–422.

**Deschamps, R.**, **Sale, S.O.**, **Chauveau, B.**, **Fierens, R.** and **Euzen, T.** (2017) The coal-bearing strata of the Lower Cretaceous Mannville Group (Western Canadian Sedimentary Basin, South Central Alberta). Part 1: Stratigraphic architecture and coal distribution controlling factors. *Int. J. Coal Geol.*, **179**, 113–129.

**Duguey, E.** (1994) Relations entre deformation, contrainte et sedimentation dans une zone pyreneenne transverse : le couloir meridien turbon-roda de isabena. implications regionales et essais de

651 modelisation analogique (pyrenees aragonaises et catalanes, espagne). These de doctorat,
652 Paris 6

653 **Duguey, E.** and **Ott d'Estevou, P.** (1991) Analyse tectonique du secteur Turbon-Roda de Isabena
654 (Pyrénées Centrales Aragonaises). *Recherche et etudes industrielles en géosciences / ELF / IGAL*.

655 **Eichenseer, H.** (1988) Facies geology of late Maestrichtian to early Eocene coastal and shallow marine
656 sediments, Tremp-Graus basin, northeastern Spain. Phdthesis, Institut und Museum für
657 Geologie und Paläontologie der Universität Tübingen

658 **Eide, C.H.**, **Howell, J.A.**, **Buckley, S.J.**, **Martinius, A.W.**, **Oftedal, B.T.** and **Henstra, G.A.** (2016) Facies
659 model for a coarse-grained, tide-influenced delta: Gule Horn Formation (Early Jurassic),
660 Jameson Land, Greenland. *Sedimentology*, **63**, 1474–1506.

661 **Enge, H.D.**, **Buckley, S.J.**, **Rotevatn, A.** and **Howell, J.A.** (2007) From outcrop to reservoir simulation
662 model: Workflow and procedures. *Geosphere*, **3**, 469–490.

663 **Galloway, W.** (1975) Process framework for describing the morphologic and stratigraphic evolution of
664 deltaic depositional system. *Soc. Econ. Paleontol. Mineral. SEPM Spec. Publ. No 31*, 127–156.

665 **Gilbert, G.K.** (1885) The Topographic Features of Lake Shores. *U.S. Government Printing Office*, 142 pp.

666 **Gozalo, M.**, **Donselaar, M.E.** and **Nio, S.D.** (1985) Eocene clastic tidal deposits in the Tremp-Graus Basin
667 (provs. of Lerida and Huesca). 215–266.

668 **Gradstein, F.M.**, **Ogg, J.G.**, **Schmitz, M.D.** and **Ogg, G.M.** (2020) Geologic Time Scale 2020. *Elsevier*,
669 1393 pp.

670 **Grasseau, N.**, **Grélaud, C.**, **López-Blanco, M.** and **Razin, P.** (2019) Forward seismic modeling as a guide
671 improving detailed seismic interpretation of deltaic systems: Example of the Eocene Sobrarbe
672 delta outcrop (South-Pyrenean foreland basin, Spain), as a reference to the analogous
673 subsurface Albian-Cenomanian Torok-Nanushuk Delta of the Colville Basin (NPRA, USA). *Mar.*
674 *Pet. Geol.*, **100**, 225–245.

675 **Guillocheau, F.**, **Quéméner, J.-M.**, **Robin, C.**, **Joseph, P.** and **Broucke, O.** (2004) Genetic
676 units/parasequences of the Annot turbidite system, SE France. *Geol. Soc. Lond. Spec. Publ.*,
677 **221**, 181–202.

678 **Hardenbol, J.**, **Thierry, J.**, **Farley, M.B.**, **Jacquin, T.**, **Graciansky, P.-C. de** and **Vail, P.R.** (1998) Mesozoic
679 and Cenozoic Sequence Chronostratigraphic Framework of European Basins. *Special*
680 *Publications of SEPM*.

681 **Harris, P.**, **Baker, E.**, **Cole, A.R.** and **Short, S.** (1993) A preliminary study of sedimentation in the tidally
682 dominated Fly River Delta, Gulf of Papua. *Cont. Shelf Res.*, **13**, 441–472.

683 **Hodgetts, D.** (2010) Collection, processing, interpretation and modelling of digital outcrop data using
684 VRGS: An integrated approach to outcrop modelling. *European Association of Geoscientists &*
685 *Engineers*, cp.

686 **Hodgetts, D.** (2013) Laser scanning and digital outcrop geology in the petroleum industry: A review.
687 *Mar. Pet. Geol.*, **46**, 335–354.

**Hori, K.**, **Saito, Y.**, **Zhao, Q.** and **Wang, P.** (2002) Architecture and evolution of the tide-dominated Changjiang (Yangtze) River delta, China. *Sediment. Geol.*, **146**, 249–264.

**Howell, J.**, **Chmielewska, M.**, **Lewis, C.**, **Buckley, S.**, **Naumann, N.** and **Pugsley, J.** (2021) Acquisition of Data for Building Photogrammetric Virtual Outcrop Models for the Geosciences using Remotely Piloted Vehicles (RPVs).

**Jimenez, M.C.** (1987) Plaéoécologie et valeurs chronostratigraphique des foraminifères benthiques dans des systèmes sédimentaires littoraux et deltaïques. Paul Sabatier

**Joseph, P.**, **Hu, L.**, **Dubrule, O.**, **Claude, D.**, **Crumeyrolle, P.**, **Lesueur, J.-L.** and **Soudet, H.** (1993) The Roda deltaic complex (Spain): from sedimentology to reservoir stochastic modelling. In: *Subsurface reservoir characterization from outcrop observations*, R. Eshard and B. Doligez, *Editions Technip*, Paris, 97–109.

**Joseph, Ph.** (1994) PROJET ETUDE DES AFFLEUREMENTS - Modélisation 3D des Grès de Roda - Volume 1 - Texte. *IFP*.

**Knaust, D.** (2017) Atlas of Trace Fossils in Well Core: Appearance, Taxonomy and Interpretation. *Springer*, 219 pp.

**Leren, B.L.S.**, **Howell, J.**, **Enge, H.** and **Martinius, A.W.** (2010) Controls on stratigraphic architecture in contemporaneous delta systems from the Eocene Roda Sandstone, Tremp-Graus Basin, northern Spain. *Sediment. Geol.*, **229**, 9–40.

**Leuven, J.R.F.W.**, **Kleinhans, M.G.**, **Weisscher, S.A.H.** and **van der Vegt, M.** (2016) Tidal sand bar dimensions and shapes in estuaries. *Earth-Sci. Rev.*, **161**, 204–223.

**Longhitano, S.G.** and **Nemec, W.** (2005) Statistical analysis of bed-thickness variation in a Tortonian succession of biocalcarenitic tidal dunes, Amantea Basin, Calabria, southern Italy. *Sediment. Geol.*, **179**, 195–224.

**Longhitano, S.G.** and **Steel, R.J.** (2017) Deflection of the progradational axis and asymmetry in tidal seaway and strait deltas: insights from two outcrop case studies. doi: 10.1144/SP444.8

**López Blanco, M.** (1996) Estratigrafía secuencial de sistemas deltaicos en cuencas de antepaís: ejemplos de Sant Llorenç del Munt, Montserrat y Roda (Paleógeno: cuenca de antepaís surpirenaica). Ph.D. Thesis, Universitat de Barcelona

**López-Blanco, M.**, **Marzo, M.** and **Muñoz, J.A.** (2003) Low-amplitude, synsedimentary folding of a deltaic complex: Roda Sandstone (lower Eocene), South-Pyrenean Foreland Basin. *Basin Res.*, **15**, 73–96.

**MacEachern, J.A.** and **Bann, K.L.** (2020) The Phycosiphon Ichnofacies and the Rosselia Ichnofacies: Two new ichnofacies for marine deltaic environments. *J. Sediment. Res.*, **90**, 855–886.

**MacEachern, J.A.**, **Bann, K.L.**, **Bhattacharya, J.P.** and **Howell, C.D., Jr.** (2005) Ichnology of Deltas: Organism Responses to the Dynamic Interplay of Rivers, Waves, Storms, and Tides. In: *River Deltas–Concepts, Models, and Examples* (Ed. L. Giosan and J.P. Bhattacharya), *SEPM Society for Sedimentary Geology*, 83, 0.

**Marques, A.**, **Horota, R.K.**, **de Souza, E.M.**, **Kupssinskü, L.**, **Rossa, P.**, **Aires, A.S.**, **Bachi, L.**, **Veronez, M.R.**, **Gonzaga, L.** and **Cazarin, C.L.** (2020) Virtual and digital outcrops in the petroleum industry: A systematic review. *Earth-Sci. Rev.*, **208**, 103260.

**Martinius, A.W.** (2012) Contrasting Styles of Siliciclastic Tidal Deposits in a Developing Thrust-Sheet-Top Basins – The Lower Eocene of the Central Pyrenees (Spain). In: *Principles of Tidal Sedimentology* (Ed. R.A. Davis and R.W. Dalrymple), *Springer Netherlands*, Dordrecht, 473–506.

**Martinius, A.W.** (1995) Macrofauna associations and formation of shell concentrations in the Early Eocene Roda Formation (southern Pyrenees, Spain). *Scr. Geol.*, **108**, 1–39.

**Martinius, A.W.** and **Van den Berg, J.H.** (2011) Atlas Of Sedimentary Structures In Estuarine and Tidally-Influenced River Deposits of the Rhine-Meuse-Scheldt System. Their Application to the Interpretation of Analogous Outcrop and Subsurface Depositional Systems. *EAGE*.

**Michaud, K.J.** (2011) Facies Architecture and Stratigraphy of Tidal Ridges in the Eocene Roda Formation, Northern Spain. Thesis

**Michaud, K.J.** and **Dalrymple, R.W.** (2016) Facies, architecture and stratigraphic occurrence of headland-attached tidal sand ridges in the Roda Formation, Northern Spain. In: *Contributions to Modern and Ancient Tidal Sedimentology* (Ed. B. Tessier and J.-Y. Reynaud), *John Wiley & Sons, Ltd*, Chichester, UK, 313–341.

**Miller, K.G.**, **Browning, J.V.**, **Schmelz, W.J.**, **Kopp, R.E.**, **Mountain, G.S.** and **Wright, J.D.** (2020) Cenozoic sea-level and cryospheric evolution from deep-sea geochemical and continental margin records. *Sci. Adv.*, **6**, eaaz1346.

**Molenaar, N.** (1990) Calcite cementation in shallow marine Eocene sandstones and constraints of early diagenesis. *J. Geol. Soc.*, **147**, 759–768.

**Molenaar, N.** and **Martinius, A.** (1996) Fossiliferous intervals and sequence boundaries in shallow marine, fan-deltaic deposits (Early Eocene, southern Pyrenees, Spain). *Palaeogeogr. Palaeoclimatol. Palaeoecol.*, **121**, 147–168.

**Molenaar, N.** and **Martinius, A.W.** (1990) Origin of nodules in mixed siliciclastic-carbonate sandstones, the Lower Eocene Roda Sandstone Member, southern Pyrenees, Spain. *Sediment. Geol.*, **66**, 277–293.

**Muñoz, J.A.** (1992) Evolution of a continental collision belt: ECORS-Pyrenees crustal balanced cross-section. In: *Thrust Tectonics* (Ed. K.R. McClay), *Springer Netherlands*, Dordrecht, 235–246.

**Musial, G.** (2006) Les hétérogénéités réservoirs liées aux surfaces stratigraphiques - Les Grès de Roda - Espagne - approche ichnologique et modélisation.

**Mutti, E.**, **Séguret, M.**, **Sgavetti, M.**, and **American Association of Petroleum Geologists** (1988) Sedimentation and deformation in the Tertiary sequences of the southern Pyrenees: field trip 7. *University of Parma*, Parma, Italy.

**Nagtegaal, P.J.C.**, **Van Vliet, A.** and **Brouwer, J.** (1983) Syntectonic coastal offlap and concurrent turbidite deposition: The Upper Cretaceous Aren sandstone in the South-Central Pyrenees, Spain. *Sediment. Geol.*, **34**, 185–218.

763 **Nijman, W.** (1998) Cyclicity and basin axis shift in a piggyback basin: towards modelling of the Eocene
764 Tremp-Ager Basin, South Pyrenees, Spain. *Geol. Soc. Lond. Spec. Publ.*, **134**, 135–162.

765 **Nijman, W.** and **Nio, S.D.** (1976) The Eocene Montañana Delta: Tremp-Graus Basin, provinces of Lerida
766 and Huesca, Southern Pyrenees, N. Spain. *Vakgroep Sedimentologie, Rijksuniveriteit Leiden-*
767 *Utrecht*, Leiden.

768 **Nio** (1976) Marine transgression as a factor in the formation of sandwave complexes.

769 **Nio, S.D.** and **Yang, C.S.** (1991) Sea-level fluctuations and the geometric variability of tide-dominated
770 sandbodies. *Sediment. Geol.*, **70**, 161–193.

771 **Olariu, C.**, **Steel, R.J.**, **Dalrymple, R.W.** and **Gingras, M.K.** (2012a) Tidal dunes versus tidal bars: The
772 sedimentological and architectural characteristics of compound dunes in a tidal seaway, the
773 lower Baronia Sandstone (Lower Eocene), Ager Basin, Spain. *Sediment. Geol.*, **279**, 134–155.

774 **Olariu, M.I.**, **Olariu, C.**, **Steel, R.J.**, **Dalrymple, R.W.** and **Martinius, A.W.** (2012b) Anatomy of a laterally
775 migrating tidal bar in front of a delta system: Esdolomada Member, Roda Formation, Tremp-
776 Graus Basin, Spain: Esdolomada tidal bar. *Sedimentology*, **59**, 356–378.

777 **Olivier, N.**, **Carpentier, C.**, **Martin-Garin, B.**, **Lathuilière, B.**, **Gaillard, C.**, **Ferry, S.**, **Hantzpergue, P.** and
778 **Geister, J.** (2004) Coral-microbialite reefs in pure carbonate versus mixed carbonate-siliciclastic
779 depositional environments: the example of the Pagny-sur-Meuse section (Upper Jurassic,
780 northeastern France). Facies. doi: 10.1007/s10347-004-0018-5

781 **Posamentier, H.W.** and **Vail, P.R.** (1988) Sequence Stratigraphy: Sequences and Systems Tract
782 Development. 571–572.

783 **Pratt, L.. J.** (1990) The Physical Oceanography of Sea Straits.

784 **Pringle, J.**, **Gardiner, A.** and **Westerman, A.** (2004) Topics: Virtual geological outcrops - fieldwork and
785 analysis made less exhaustive? *Geol. Today*, **20**, 67–71.

786 **Puga-Bernabéu, Á.** and **Aguirre, J.** (2017) Contrasting storm- versus tsunami-related shell beds in
787 shallow-water ramps. *Palaeogeogr. Palaeoclimatol. Palaeoecol.*, **471**, 1–14.

788 **Pugh, D.T.** (1987) Tides, surges and mean sea level.

789 **Puigdefabregas, C.**, **Samso, J.M.**, **Serra-Kiel, J.** and **Tosquella, J.** (1985) Facies analysis and faunal
790 assemblages of the Roda Sandstone Formation, Eocene of the Southern Pyrenees. 639–642.

791 **Puigdefàbregas, C.** and **Souquet, P.** (1986) Tecto-sedimentary cycles and depositional sequences of the
792 Mesozoic and Tertiary from the Pyrenees. *Tectonophysics*, **129**, 173–203.

793 **Racey, A.** (2001) A Review of Eocene Nummulite Accumulations: Structure, Formation and Reservoir
794 Potential. *J. Pet. Geol.*, **24**, 79–100.

795 **Reynaud, J.**, **J.-Y** and **Dalrymple, R.** (2012) Shallow-Marine Tidal Deposits. In: *Principles of Tidal*
796 *Sedimentology*, 335–369.

797 **Reynolds, A.D.** (1999) Dimensions of Paralic Sandstone Bodies. *AAPG Bull.*, **83**, 211–229.

**Rubi, R.**, **Rohais, S.**, **Bourquin, S.**, **Moretti, I.** and **Desaubliaux, G.** (2018) Processes and typology in Gilbert-type delta bottomset deposits based on outcrop examples in the Corinth Rift. *Mar. Pet. Geol.*, **92**, 193–212.

**Schmitz, J.**, **Deschamps, R.**, **Joseph, P.**, **Doligez, B.**, **Jardin, A.** and **Lerat, O.** (2014) From 3D photogrammetric outcrop models to reservoir models : An integrated modelling workflow.

**Serra-Kiel, J.**, **Canudo, J.I.**, **Dinares, J.**, **Molina, E.**, **Ortiz, N.**, **Pascual, J.O.**, **Samsó, J.M.** and **Tosquella, J.** (1994) Cronoestratigrafía de los sedimentos marinos del Terciario inferior de la Cuenca de Graus-Tremp (Zona Central Surpirenaica). *Rev. Soc. Geológica Esp.*, **7**, 273–297.

**Shchepetkina, A.**, **Gingras, M.K.**, **Mángano, M.G.** and **Buatois, L.A.** (2019) Fluvio-tidal transition zone: Terminology, sedimentological and ichnological characteristics, and significance. *Earth-Sci. Rev.*, **192**, 214–235.

**Steel, R.J.**, **Carvajal, C.**, **Petter, A.L.** and **Uroza, C.** (2008) Shelf and Shelf-Margin Growth in Scenarios of Rising and Falling Sea Level. In: *Recent Advances in Models of Siliciclastic Shallow-Marine Stratigraphy* (Ed. G.J. Hampson, R.J. Steel, P.M. Burgess, and R.W. Dalrymple), *SEPM Society for Sedimentary Geology*, 90, 0.

**Tavani, S.**, **Corradetti, A.**, **Mercuri, M.** and **Seers, T.** (2024) VIRTUAL OUTCROP MODELS OF GEOLOGICAL STRUCTURES: From the construction of photogrammetric 3D models to their application towards the analysis of geological structures, 1st edn. *Società Geologica Italiana*.

**Thomas, H.**, **Brigaud, B.**, **Blaise, T.**, **Saint-Bezar, B.**, **Zordan, E.**, **Zeyen, H.**, **Andrieu, S.**, **Vincent, B.**, **Chirol, H.**, **Portier, E.** and **Mouche, E.** (2021) Contribution of drone photogrammetry to 3D outcrop modeling of facies, porosity, and permeability heterogeneities in carbonate reservoirs (Paris Basin, Middle Jurassic). *Mar. Pet. Geol.*, **123**, 104772.

**Tinterri, R.** (2007) The Lower Eocene Roda Sandstone (South-Central Pyrenees): an Example of a Flood-Dominated River-Delta System in a Tectonically Controlled Basin. *Riv. Ital. Paleontol. E Stratigr.*, **113**, 223–255.

**Tonkin, N.S.** (2012) Deltas. In: *Developments in Sedimentology*, *Elsevier*, 64, 507–528.

**Torricelli, S.**, **Knezaurek, G.** and **Biffi, U.** (2006) Sequence biostratigraphy and paleoenvironmental reconstruction in the Early Eocene Figols Group of the Tremp–Graus Basin (south-central Pyrenees, Spain). *Palaeogeogr. Palaeoclimatol. Palaeoecol.*, **232**, 1–35.

**Tosquella, J.** (1988) Estudi Sedimentògic i Biostratigràfic de la Formacio Gresos de Roda (Eocè, Conca Tremp-Graus). Msc Thesis, Universitat de Barcelona

**Uroza, C.A.** (2008) Processes and architectures of deltas in shelf-break and ramp platforms : examples from the Eocene of West Spitsbergen (Norway), the Pliocene paleo-Orinoco Delta (SE Trinidad), and the Cretaceous Western Interior Seaway (S. Wyoming & NE Utah).

**Vail, P.R.**, **Mitchell, R.M.**, **Sangree, J.D.** and **Thompson, S.** (1975) Eustatic Cycles from Seismic Data for Global Stratigraphic Analysis. **18**, 16–16.

**Vail, P.R.**, **Mitchum, R.M., Jr.** and **Thompson, S., III** (1977) Seismic Stratigraphy and Global Changes of Sea Level, Part 4: Global Cycles of Relative Changes of Sea Level. In: *Seismic Stratigraphy — Applications to Hydrocarbon Exploration* (Ed. C.E. Payton), *American Association of Petroleum Geologists*, 26, 0.

**Van Wagoner, J.C.**, **Posamentier, H.W.**, **R. M. Mitchum**, **Vail, P.R.**, **Sarg, J.F.**, **Loutit, T.S.** and **Hardenbol, J.** (1988) An Overview of the Fundamentals of Sequence Stratigraphy and Key Definitions.

**Vaucher, R.**, **Musajo, C.**, **Spangenberg, J.E.**, **Poyatos-Moré, M.**, **Zeeden, C.**, **Puigdefàbregas, C.**, **Prieur, M.**, **Castelltort, S.** and **Adatte, T.** (2024) Sediment supply variation control on Lower Eocene delta sequences (Tremp Basin, Spain). Geology. doi: 10.1130/G52548.1

**Vincent, S.J.** and **Elliott, T.** (1997) Long-lived transfer-zone paleovalleys in mountain belts; an example from the Tertiary of the Spanish Pyrenees. *J. Sediment. Res.*, **67**, 303–310.

**Westerhold, T.**, **Marwan, N.**, **Drury, A.J.**, **Liebrand, D.**, **Agnini, C.**, **Anagnostou, E.**, **Barnet, J.S.K.**, **Bohaty, S.M.**, **De Vleeschouwer, D.**, **Florindo, F.**, **Frederichs, T.**, **Hodell, D.A.**, **Holbourn, A.E.**, **Kroon, D.**, **Lauretano, V.**, **Littler, K.**, **Lourens, L.J.**, **Lyle, M.**, **Pälike, H.**, **Röhl, U.**, **Tian, J.**, **Wilkens, R.H.**, **Wilson, P.A.** and **Zachos, J.C.** (2020) An astronomically dated record of Earth's climate and its predictability over the last 66 million years. *Science*, **369**, 1383–1387.

**Willis, B.** (2005) Deposits of Tide-Influenced River Deltas. In: *SEPM Spec. Publ.*, 83,

**Yang, C.-S.** and **Nio, S.-D.** (1989) An ebb-tide delta depositional model—a comparison between the modern Eastern Scheldt tidal basin (southwest Netherlands) and the Lower Eocene Roda Sandstone in the southern Pyrenees (Spain). *Sediment. Geol.*, **64**, 175–196.

**Zachos, J.**, **Pagani, M.**, **Sloan, L.**, **Thomas, E.** and **Billups, K.** (2001) Trends, Rhythms, and Aberrations in Global Climate 65 Ma to Present. *Science*, **292**, 686–693.

**Zavala, C.**, **Arcuri, M.**, **Zorzano, A.**, **Trobbiani, V.**, **Torresi, A.** and **Irastorza, A.** (2024) Deltas: New paradigms. *Depositional Rec.*, **0**, 1–37.

# 10 Figure captions

**Figure 1** - A) Structural map of the south-Pyrenean Basin (modified after López-Blanco et al. (2003) and Coll et al. (2013)), the red star refers to the study area location; JB = Jaca Basin, AB = Ainsa Basin, GTB = Graus-Tremp Basin. / B) paleogeographic map of the late Ypresian times synthesized from Castelltort et al. (2017), Chanvry et al. (2018) and Vaucher et al. (2024), Razin, unpublished.

**Figure 2** - A) Simplified geological map of the Graus-Tremp Basin (modified after Serra-Kiel et al. (1994) with faults (dark red) and measured stratigraphic sections Serraduy South (SS) and Codoñeras (C). The dotted rectangle corresponds to the study area and location of Figure 4. / B) Chrono-litho-stratigraphic diagrams of the Tremp-Graus-Ainsa Basin during the Ypresian times. Polarity chrons are from the GTS 2020 (Gradstein et al., 2020). ; 1.) Planktonic foraminifera biozones from Berggren et al. (1995). ; 2.) Calcareous nannofossils zones are from Berggren et al. (1995), Backman et al. (2012) and Agnini et al. (2017). ; 3.) Shallow Benthic Zones are from Hardenbol et al. (1998) and updated by GTS2020 Paleogene chapter group. ; Offsets from long-term curve are from Hardenbol et al. (1998). ; Sea-level curve is from Miller et al. (2020). ; Benthic δ18O curve is from Westerhold et al. (2020); Lithostratigraphic schemes from Nio & Yang (1991), Serra-Kiel et al. (1994) and López-Blanco et al., (2003). 4.) Lithostratigraphic schemes from Mutti et al. (1988); 5.) Lithostratigraphic schemes from Tinterri (2007). The background colours correspond to the lithostratigraphic map modified after Serra-Kiel et al. (1994).

**Figure 3** - Cross-section of the Roda Sandstone modified from López-Blanco et al. (2003) correlated with 1.Geomagnetic polarity from Bentham & Burbank (1996) 2. Proposition of system tracts of a 3rd order depositional sequence 3. system tracts of a 3rd order depositional sequence after Nio & Yang (1991) ; relative sea-level evolution from Miller et al. (2020), 4. Lithostratigraphic scheme of the Roda Sandstone Formation divided into two members (Roda Sandstone Member and Esdolomada Member) from Nio & Yang (1991). The present study is focused on the Y sandbody.

**Figure 4** – Satellite image of the study area, showing field and drone data; stratigraphic sections are Zipaguerne 1 (Z1), Zipaguerne 2 (Z2), Puebla East (PE), El Villar (EV), El Villar South (EVS), Meander 1-4 (M1-4), Road-cut (RC), Las Forcas 1-5 (LF 1-5), North Road-cut (NRC) and Puebla North-West (PNW). Points of interest correspond to locations where measurements, photographs, or panorama were acquired but no vertical sections.

**Figure 5** - Workflow applied for the present study.

**Figure 6** - Outcrop and core features of facies association FA 1 “Deltaic mouth bar topsets”. Locations as indicated in Fig. 4. A) Highly bioturbated medium-grained sandstone with few benthic foraminifera but no nummulites. From cored section RODA 7 (depth: 26,5 m). Source: TotalEnergies. B) Grey silty sandstone enriched in shells (F1a). From log Meander 1 (see Supplementary data; height: 1 m). Pen (13,5 cm) for scale. C) Very coarse-grained sandstone or granules with erosive base and fining-up trend (F1b). From cored section RODA 3 (depth: 35 m). Source: TotalEnergies. D) Highly bioturbated silty sandstone enriched in shells (F1a). The shells are scattered in a silty matrix. From Point of Interest 2. Pen (13,5 cm) for scale. E) Very coarse-grained sandstone with trough bedding (F1b) at the top of a delta mouth bar, forming the delta lobe topsets. From log Zipaguerne 1 (see Supplementary data; height: 25,5 m). Hammer (33 cm) for scale.

**Figure 7** - Outcrop and core features of facies association FA 2 “Deltaic mouth bar foresets”. Locations as indicated in Fig. 4. A) Capture of the Digital Outcrop Model in between the Puebla East and Zipaguerne 2 vertical sections area. The clinoforms of the deltaic lobes 1 and 2 are highlighted and they are composed of facies associations FA 2 deposits. B) Medium-grained sandstone with planar cross-bedding (F2b). The laminae are parallel to the beds. From cored section RODA 1 (depth: 53,5 m). C) Ophiomorpha (Oph.) fossil trace in medium to coarse-grained sandstone with trough bedding (F2a) in the uppermost part of the delta lobe foresets. From cored section RODA 4 (depth: 8,5 m). D) Medium to coarse-grained sandstone with trough cross-bedding (F2a) dipping to the west. From log Roadcut (see Supplementary data; height: 52 m). Hammer (33 cm) for scale. E) Medium to coarse-grained sandstone with planar cross-bedding (F2b) in a decametre-thick bedset. the stratification appears tabular because the outcrop cuts the progradation direction orthogonally. From log Roadcut (see Supplementary data; height: 38 to 42 m). Jacob staff (120 cm) for scale. F) Medium-grained sandstone with no sedimentary structure visible (F2d). Millimetre-sized wood and shell debris are dispersed. From cored section RODA 1 (depth: 60,1 m). G) Compound bedding in a mouth bar foresets (F2c) formed by tidal currents reworking. From log Zipaguerne 1 (see Supplementary data; height: 19 m). H) Low angles between the laminae and the beds form the compound bedding (F2c) that reflects the reworking of tidal currents. The different colours can indicate a different cementation. From cored section RODA 4 (depth: 12,7 m). Source: TotalEnergies. I) Metre-high simple tidal dune formed by dominant tidal current (paleocurrent toward N320°) on facies F2c deposits. From Point of Interest 6. J) Skolithos (Sk.) trace fossils in tidal dune sets (F2e). Quartz grains are visible to the naked eye. From log Las Forcas 6 (see Supplementary data; height: 6 to 6,4 m). Card (8,2 cm long, 5 cm wide) for scale. K) Medium to coarse-grained sandstone in bundles dipping in opposite directions, illustrating bidirectionality in tidal bars (F2e). The beds are intercalated with finer argillaceous deposits. From log Puebla North-West (see Supplementary data; height: 11 m). Compass (17 cm) for scale. L) Bioturbated silty clay in the master

bedding deposits (F2f) intercalated in between compound dunes composing a tidal bar. From log Las Forcas 6 (see Supplementary data; height: 2 m). Card (8,2 cm long, 5 cm wide) for scale. M) Interpreted panorama of the Las Forcas outcrop showing a tidal bar formed by tidal currents reworking and then covered by compound cross-bedding deposits (F2c) deposited during the next deltaic lobe progradation phase.

**Figure 8** - Outcrop and core features of facies association FA 3 "Deltaic mouth bar bottomsets". Locations as indicated in Fig. 4. A) Medium-grained sandstone with current ripples (F3a) and grey silty fine-grained sandstone with mud drapes (F3b) characteristic of delta lobes bottomsets deposits (FA 3). From cored section RODA 7 (depth: 48,45 to 49,3 m). Source: TotalEnergies. B) Thalassinoides (Th.) fossil traces in medium-grained sandstone where horizontal burrows predominate (FA 4). From Point of Interest 4. Card (8,2 cm long, 5 cm wide) for scale. C) Highly bioturbated siltstone (F3b). The oxidized nodules probably formed around dissolved brachiopod shells. From log Las Forcas 6. Card (8,2 cm long, 5 cm wide) for scale. D) Very fine to fine-grained sandstone with current ripples and occasional mud drapes in decimetre-thick low-angle beds (F3b) characteristic of delta lobes bottomsets deposits. From Point of Interest 4. Pen (13,5 cm) for scale. E) Metre-sized Rosselia (Rs.) fossil trace in sigmoidal tidal bundles in a tidal bar (F3c). From log Roadcut (see Supplementary data; height: 12 m). F) Coarse-grained sandstone bundles showing reactivation surfaces (F3c) and with argillaceous intercalations characteristic of tidal sand bodies (F3d). From cored section RODA 1 (depth: 62 m). Source: TotalEnergies. G) Tidal dunes with sigmoidal cross-bedding (F3c) intercalated by clay couplets (F3d) and composing a tidal bar. From Point of Interest 5. H) Interpreted tidal bar deposits with tidal bundles thicknesses showing the neap-spring water cycles and clay couplets. From Point of Interest 3.

**Figure 9** - Outcrop and core details features of facies association FA 4 "Low-energy mixed distal deposits" and FA 5 "Fine pro-delta deposits". A) Thalassinoides (Th.) and Ophiomorpha (Oph.) fossil traces in bioturbated medium-grained sandstone (F4a) with a fracture filled with calcite. From cored section RODA 1 (depth: 41 m). B) Palaeophycus (Pa.) and Siphonichnus (Si.) trace fossils in intensely bioturbated medium-grained sandstone lacking visible sedimentary structures (F4b). From cored section RODA 1 (depth: 72,4 m). C) Bioclastic wackestone enriched in foraminifera (nummulites, few alveolina, orbitolites or milioles) and millimetre to pluri-centimetre-sized bioclasts (bivalves, gastropods, corals) (F4c). From cored section RODA 1 (depth: 67,5 m). D) Contorted heavily bioturbated fine sandstone (F4a) laying on distal grey marls (F5b) at the base of the Y sand body. From log Roadcut (see Supplementary data; height: 6 to 8 m). Hammer (33 cm) for scale. E) Shell lag bed in grey marls (F5a). From cored section RODA 5 (depth: 57 m). F) Grey marls with either dispersed nummulite or agglomerated characteristic of fine pro-delta deposits (F5b). From cored section RODA 7 (depth: 59,1 m). Source: TotalEnergies. G) Palaeophycus (Pa.) trace fossil in fine pro-delta nummulitic marls (F5b). From cored section RODA 7 (depth: 59,1 m). H) Silty to shaly grey marls enriched in mussels and foraminifera (mostly nummulites) (F5b). Note the significant alteration of this type of fine deposit. From Point of Interest 5. Hammer (33 cm) for scale.

**Figure 10** - Reference core RODA 1 (Figure 4 for location) with the interpreted Maximum Regressive Surfaces and Maximum Flooding Surfaces delimiting the seven deltaic lobes groups into three sequences Y1, Y2 and Y3.

**Figure 11** - A) Photogrammetric model of the Roadcut outcrop (see RC in Figure 4); B) Interpreted DOM with facies property, Maximum Regressive surfaces (solid black lines), Maximum Flooding Surfaces (dotted black lines). Y3 and Y4 correspond to the sub-units of the Y sandbody defined by López-Blanco et al. (2003). The glyphs are the sedimentary dips, representing the potential paleocurrent directions in the rose charts underneath. Blue data on the rose diagrams are dip measured on deltaic clinoform bedsets, and pink data are dip measured on tidal dunes foresets. These values must be considered

cautiously because they are not corrected for regional dip (8° toward N170°). The dark data plotted in the background of the diagrams are from Leren et al. (2010) (black = tidal currents, grey = delta lobe currents).

**Figure 12** - A) Photogrammetric model of the El Villar outcrop (see EV and EVS in Figure 4); B) Interpreted DOM with facies property, Maximum Regressive surfaces (solid black lines), Maximum Flooding Surfaces (dotted black lines). The glyphs are the sedimentary dips, representing the potential paleocurrent directions in the rose charts underneath. Blue data on the rose diagrams are dip measured on deltaic clinoform bedsets, and pink data are dip measured on tidal dunes foresets. These values must be considered cautiously because they are not corrected for regional dip (8° toward N170°). The dark data plotted in the background of the diagrams are from Leren et al. (2010) (black = tidal currents, grey = delta lobe currents).

**Figure 13** – A) Photogrammetric model of the Las Forcas outcrop (see LF1-5 in Figure 4); B) Interpreted DOM with facies property, Maximum Regressive surfaces (solid black lines), Maximum Flooding Surfaces (dotted black lines). The glyphs are the sedimentary dips, representing the potential paleocurrent directions in the rose charts underneath. C to E) Blue data on the rose diagrams are dip measured on deltaic clinoform bedsets, and pink data are dip measured on tidal dunes foresets. These values must be considered cautiously because they are not corrected for regional dip (8° toward N170°). The dark data plotted in the background of the diagrams are from Leren et al. (2010) (black = tidal currents, grey = delta lobe currents).

**Figure 14** - Cross-section 1 with lobes and facies interpretation

**Figure 15** - Cross-section of the deltaic lobe 5 illustrating vertical facies successions lateral facies transitions from a proximal pole (Zipaguerne 1) at the north-east of the study area to the distal pole (RODA 7). See Figure 13 for cross-section location.

**Figure 16** – Maps of interpreted delta lobes with corresponding facies and paleocurrents measurements. The black line on Lobe 5 map is the cross-section from Figure 21.

**Figure 17** - A) Pie charts from the different zones of the interpreted DOM showing the evolution of the facies proportions in the Y sandbody. B) Pie chart of the facies proportions in the overall interpreted DOM.

**Figure 18** – Crossplot of dimensional data for delta lobes from this study, literature data (Reynolds, 1999) and archive data about the Roda sandstone Y sandbody (Joseph et al., 1993; Joseph, 1994).

**Figure 19** - Box plot of the estimated water depths for facies F2a, F2b, F2c and facies associations FA3 and FA4 based on measurements on the DOM. A) case with water depth for reference F2a points = -5 m; B) case with water depth for reference F2a points = -10 m; C) case with water depth for reference F2a points = -15m. Water depth = 0 m is the Mean Sea Level (MSL)

**Figure 20** - Depositional models for A) Regressive setting; B) Transgressive setting.

**Figure 21** - 'Synthesis' with characteristics of the two different depositional systems during high-frequency cycles. During transgression, the restricted sediment influx results in the retrogradation of the delta system and formation of tidal dunes (1) large tidal bars (4) caused by tidal reworking. During regression, the hyperthermal event amplifies the supply to the basin, resulting in the progradation of the delta system with delta lobe progradation. Tidal reworking is still present, forming tidal dunes (1), compound bedding in the lobe foresets (2) or small extent tidal bars (3)

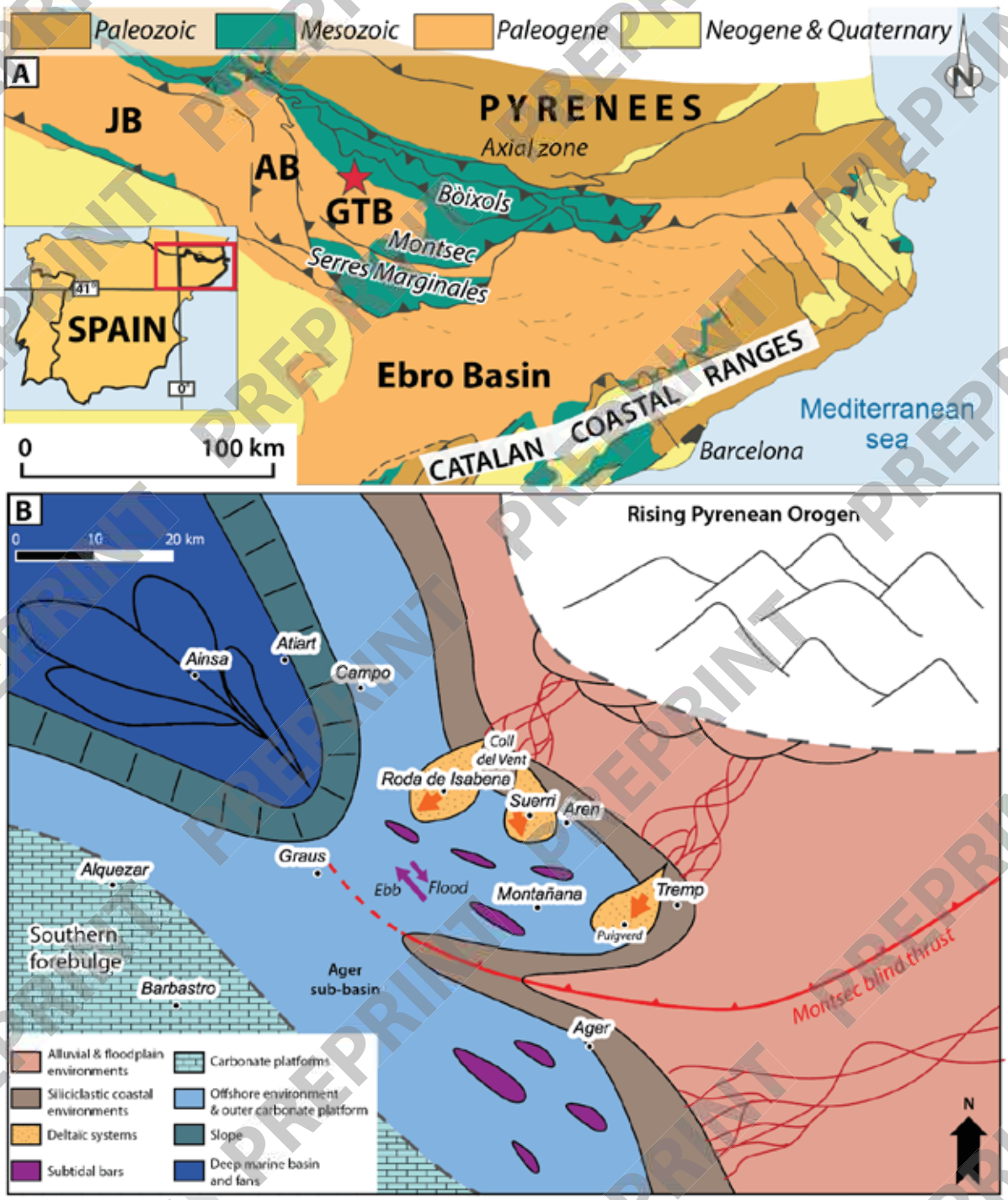


1010

1011 *Figure 1*

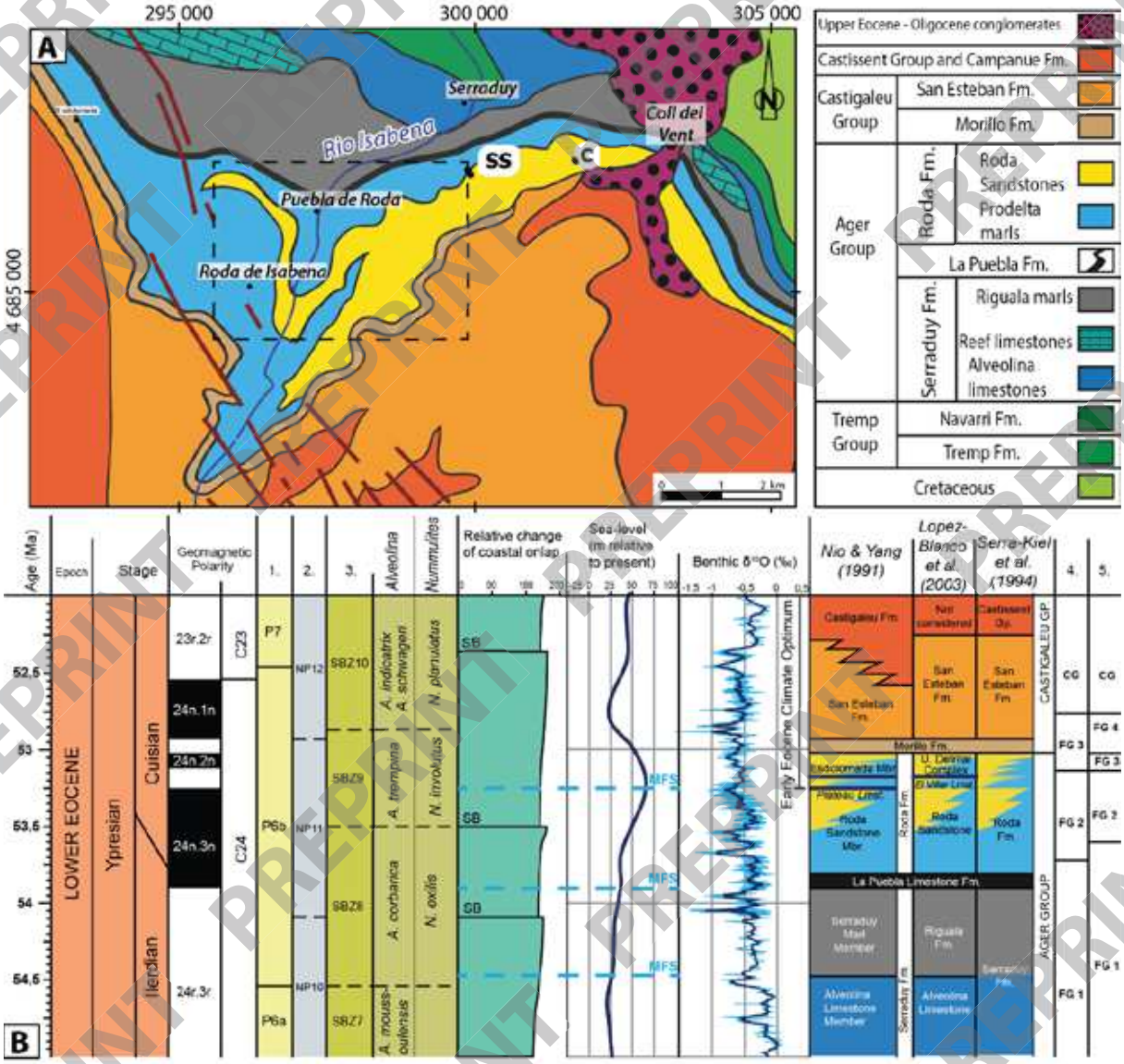


1012

1013 *Figure 2*

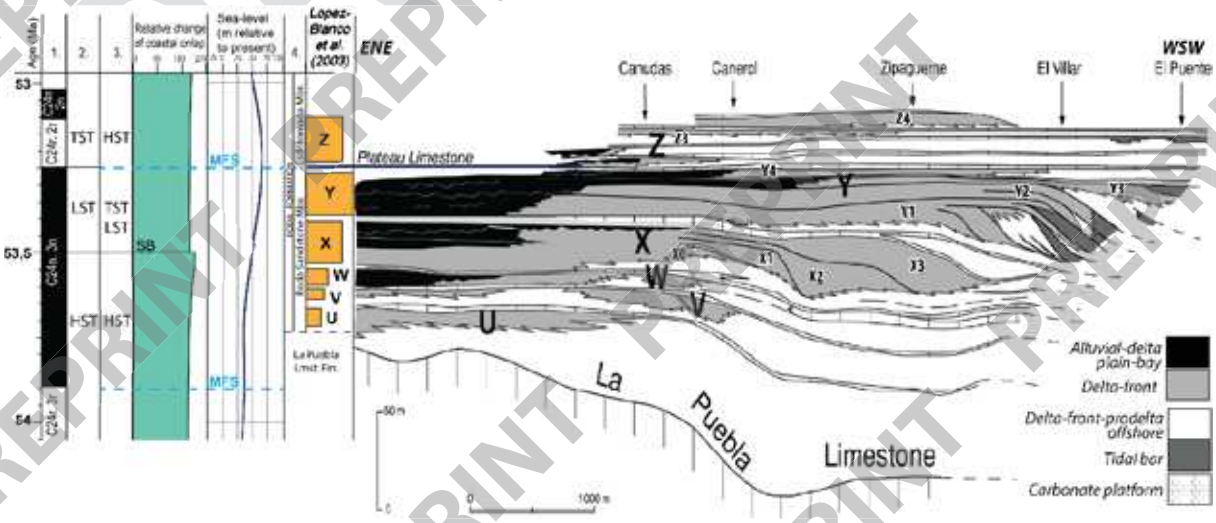


1014

1015 *Figure 3*

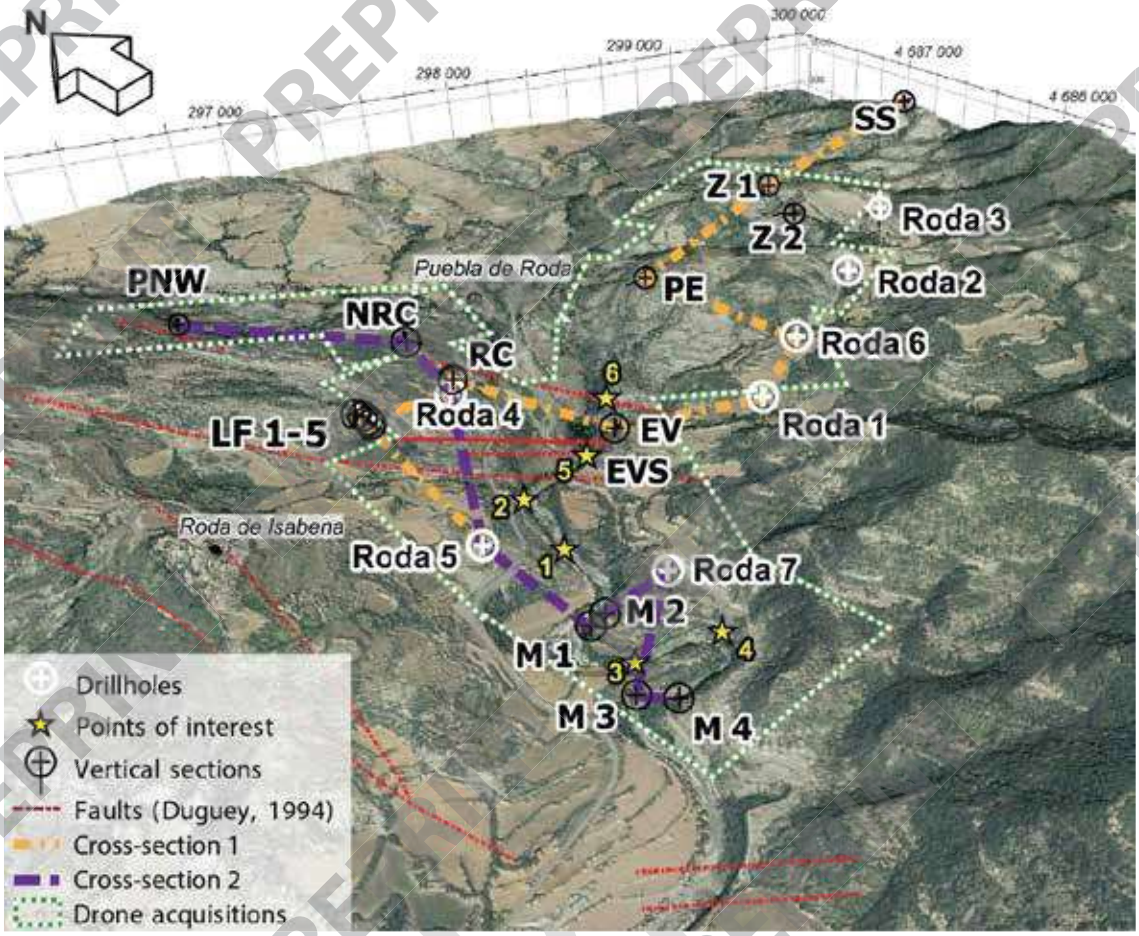


1016

1017 *Figure 4*

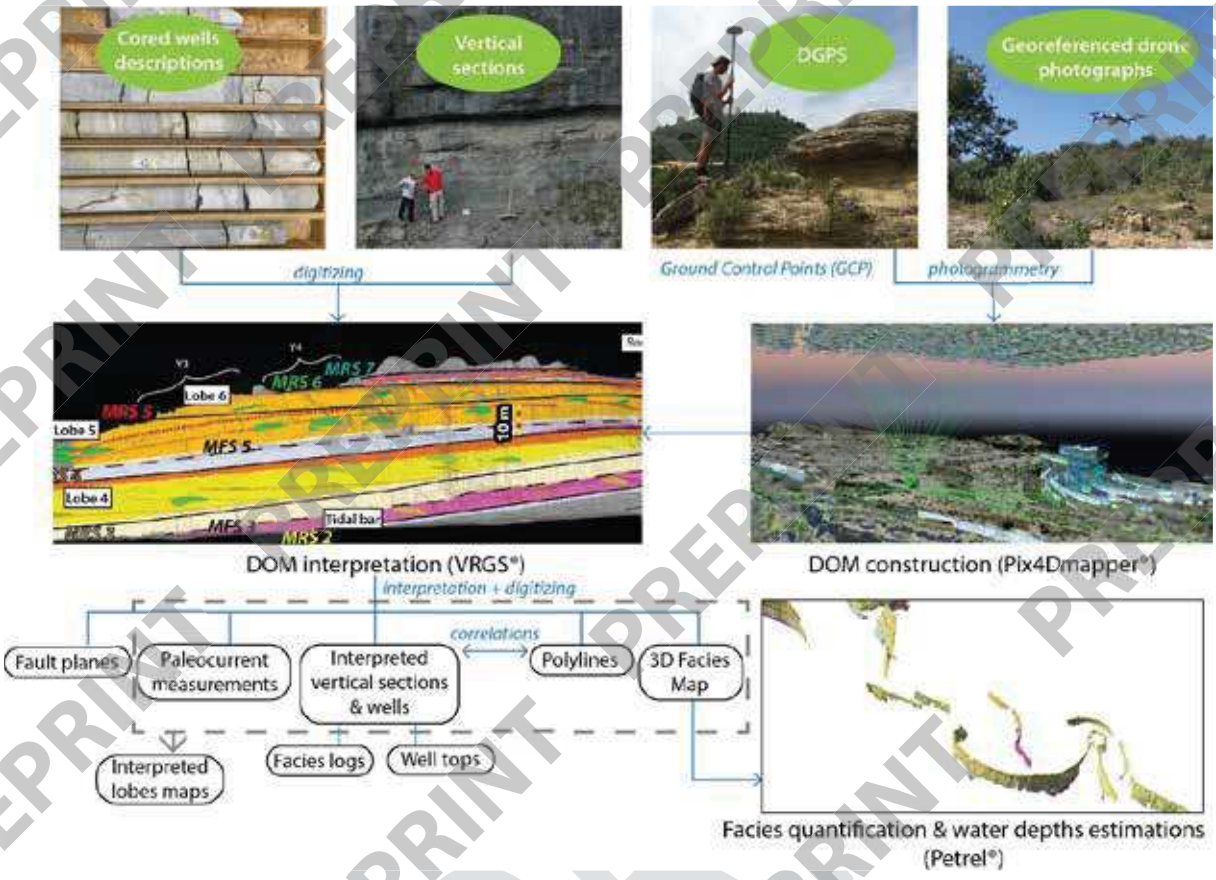


1018
1019 *Figure 5*

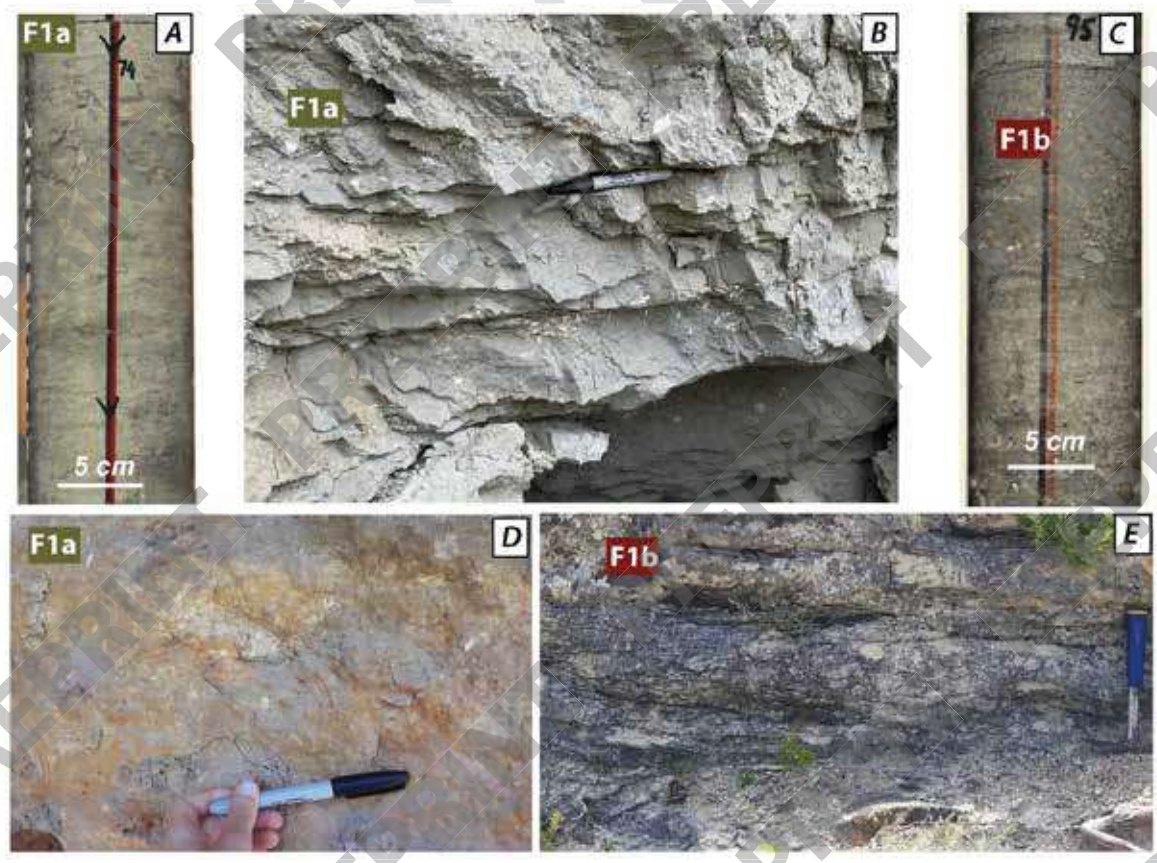


1020
1021 *Figure 6*

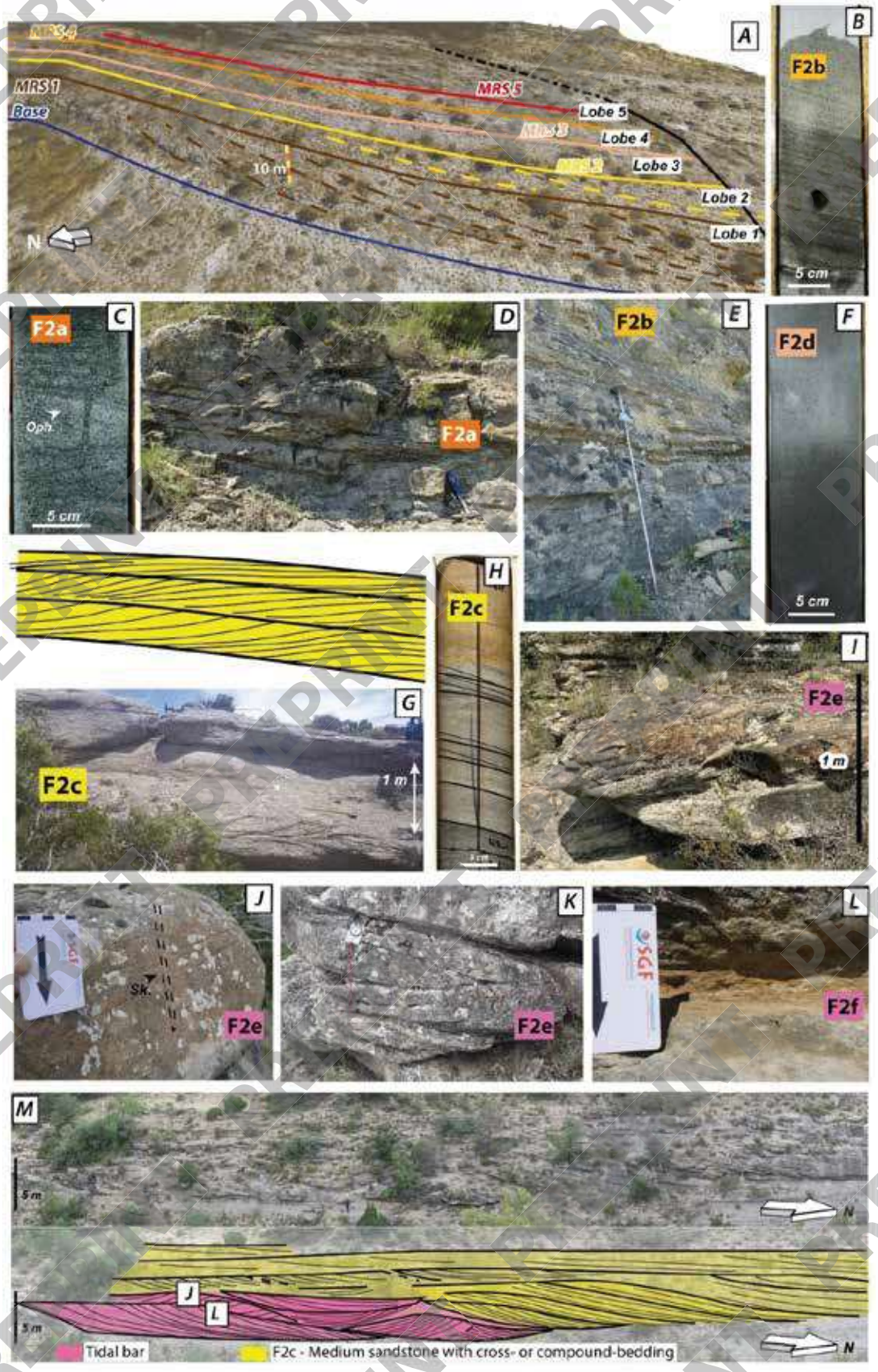


1022

1023 *Figure 7*

1024

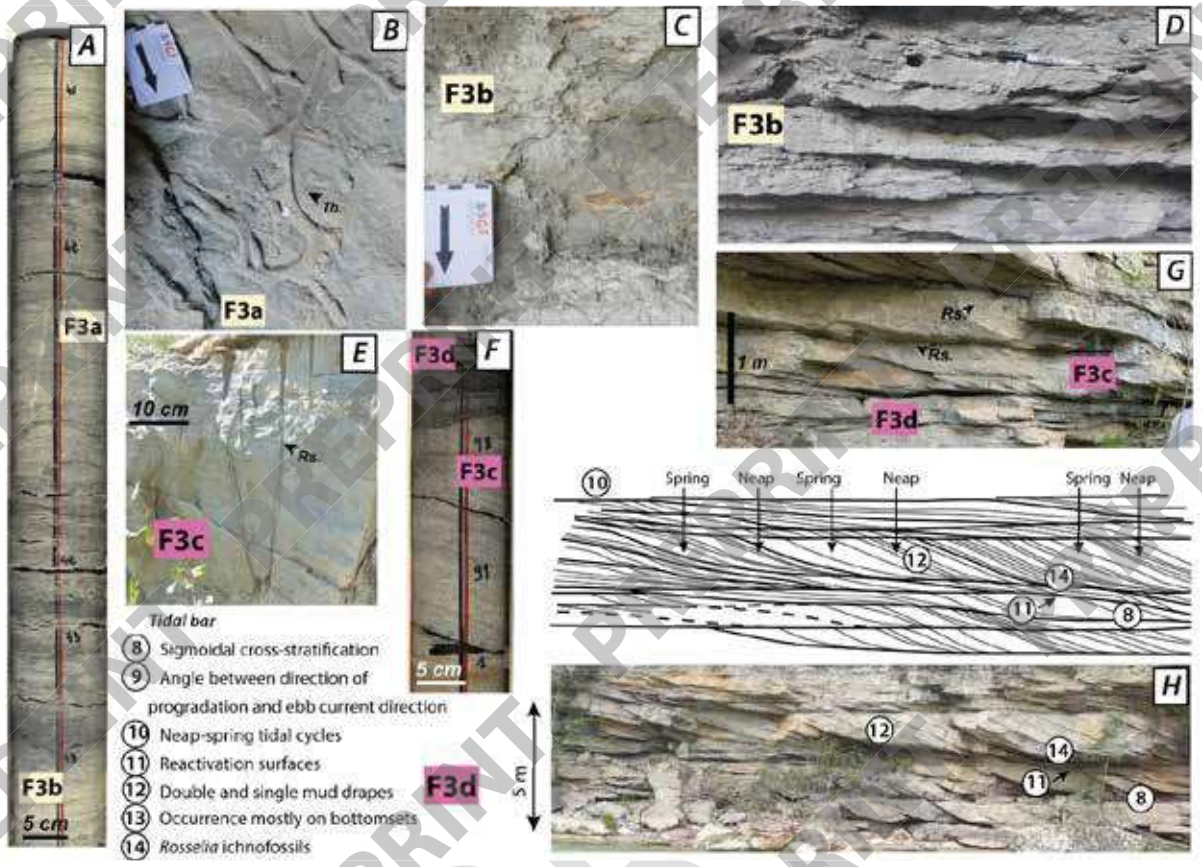


1025

1026 *Figure 8*

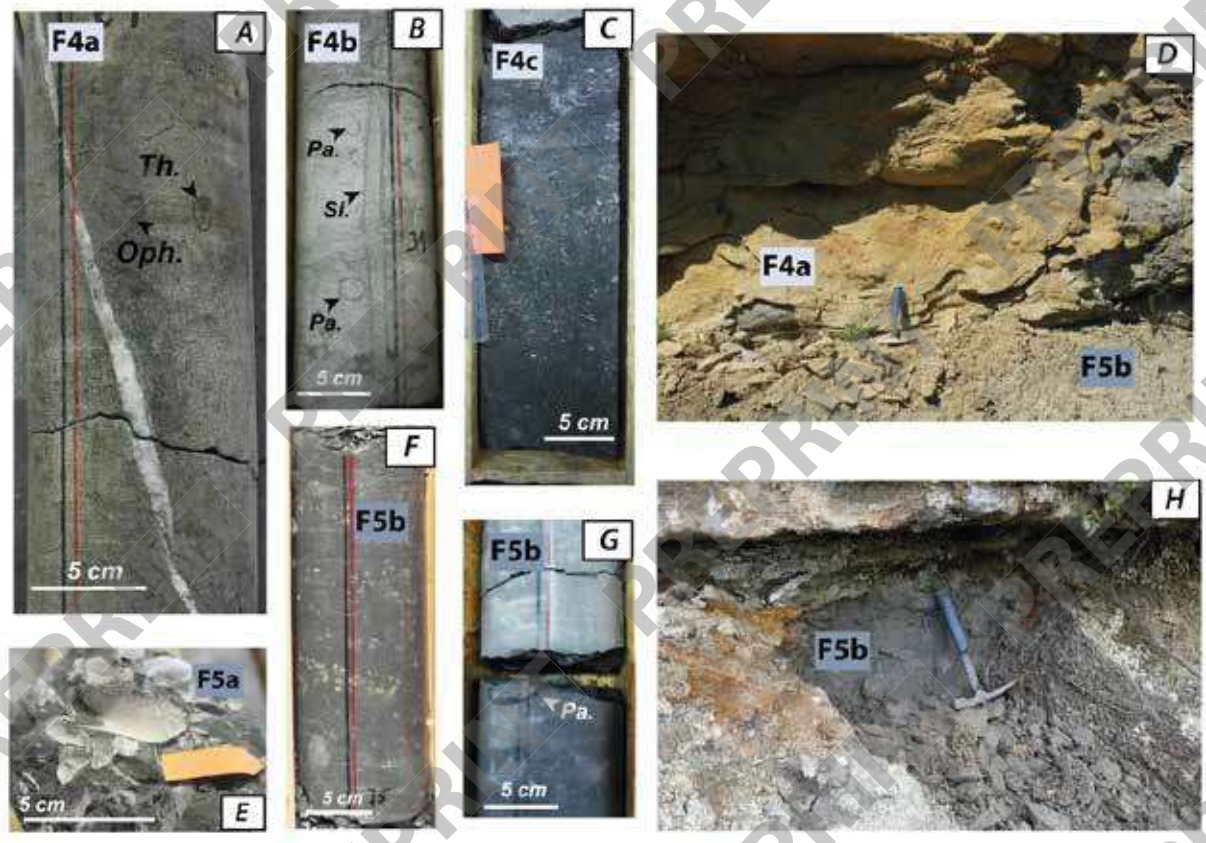


1027

1028 *Figure 9*

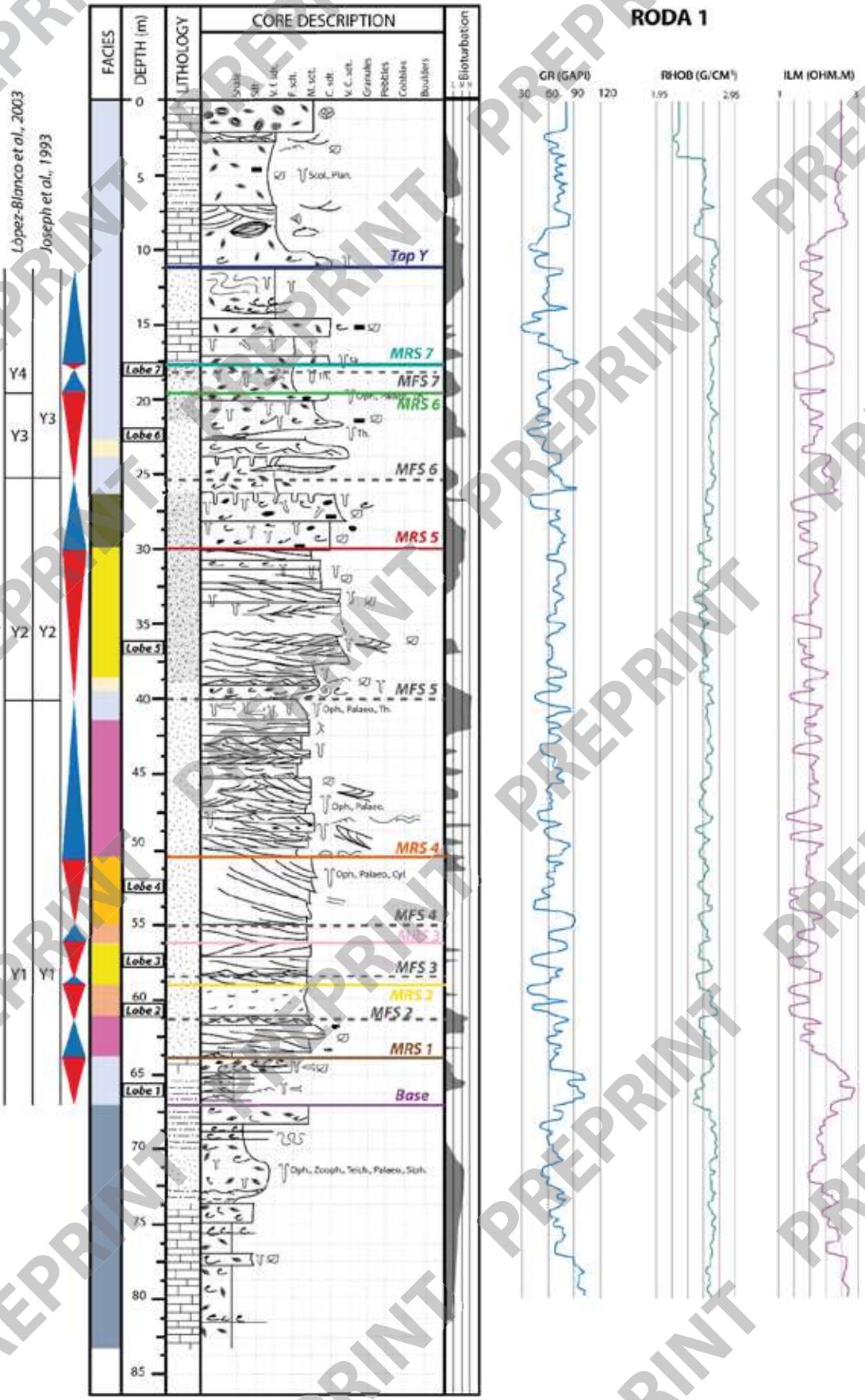


1029

1030 *Figure 10*

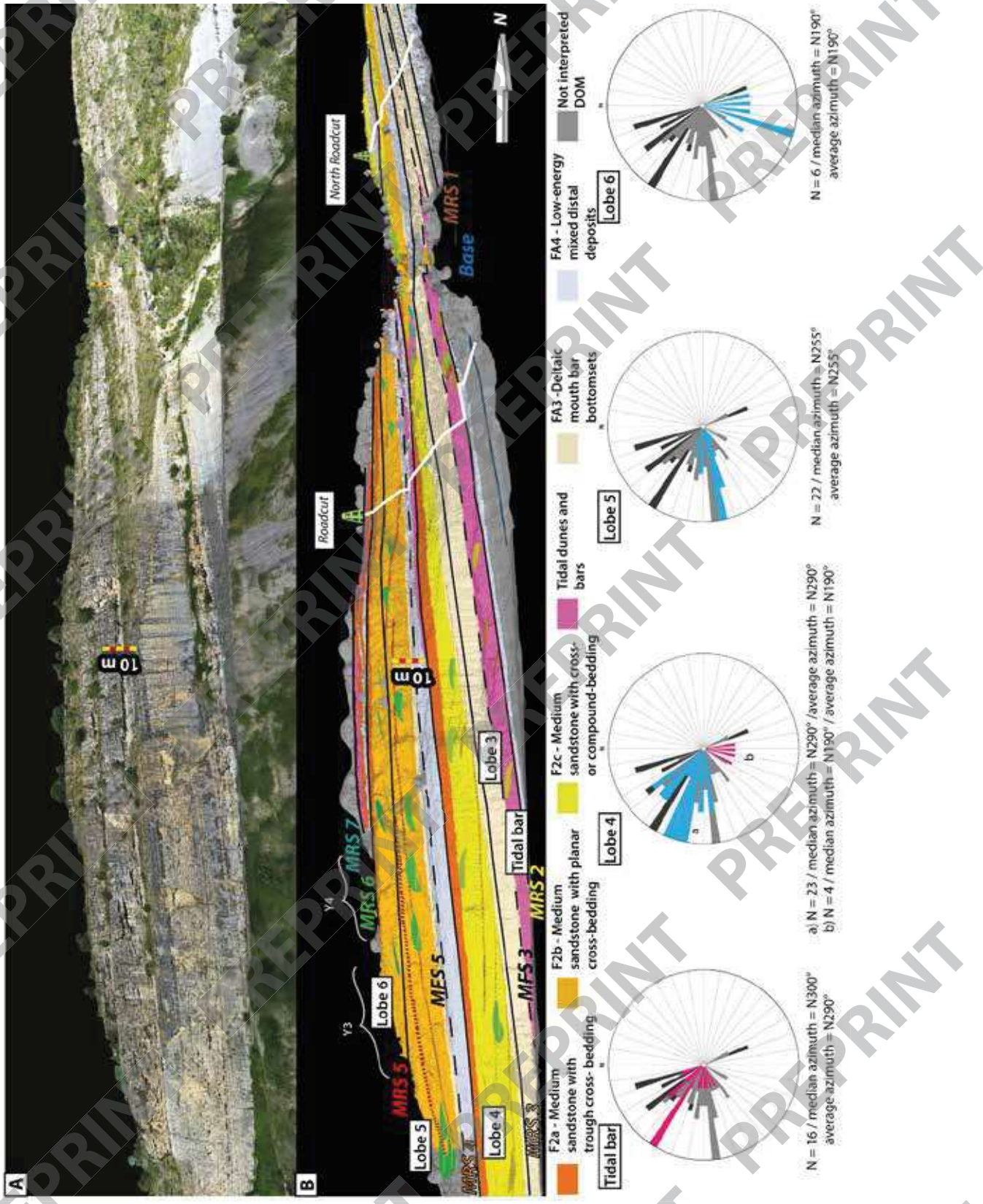
A
B
10 m
10 m
North Roadcut
Roadcut
N
MRS 1
Base
MRS 2
MRS 3
MES 3
MES 5
MRS 5
MRS 6
MRS 7
Y3
Y4
Lobe 5
Lobe 6
Lobe 4
Lobe 3
Tidal bar
F2a - Medium sandstone with trough cross- bedding
F2b - Medium sandstone with planar cross-bedding
F2c - Medium sandstone with cross- or compound-bedding
Tidal dunes and bars
FA3 -Deltaic mouth bar bottomsets
FA4 - Low-energy mixed distal deposits
Not interpreted DOM
Tidal bar
Lobe 4
Lobe 5
Lobe 6
a
b
N = 16 / median azimuth = N300°
average azimuth = N290°
a) N = 23 / median azimuth = N290° /average azimuth = N290°
b) N = 4 / median azimuth = N190° / average azimuth = N190°
N = 22 / median azimuth = N255°
average azimuth = N255°
N = 6 / median azimuth = N190°
average azimuth = N190°

*Figure 11*

1033
1034 *Figure 12*

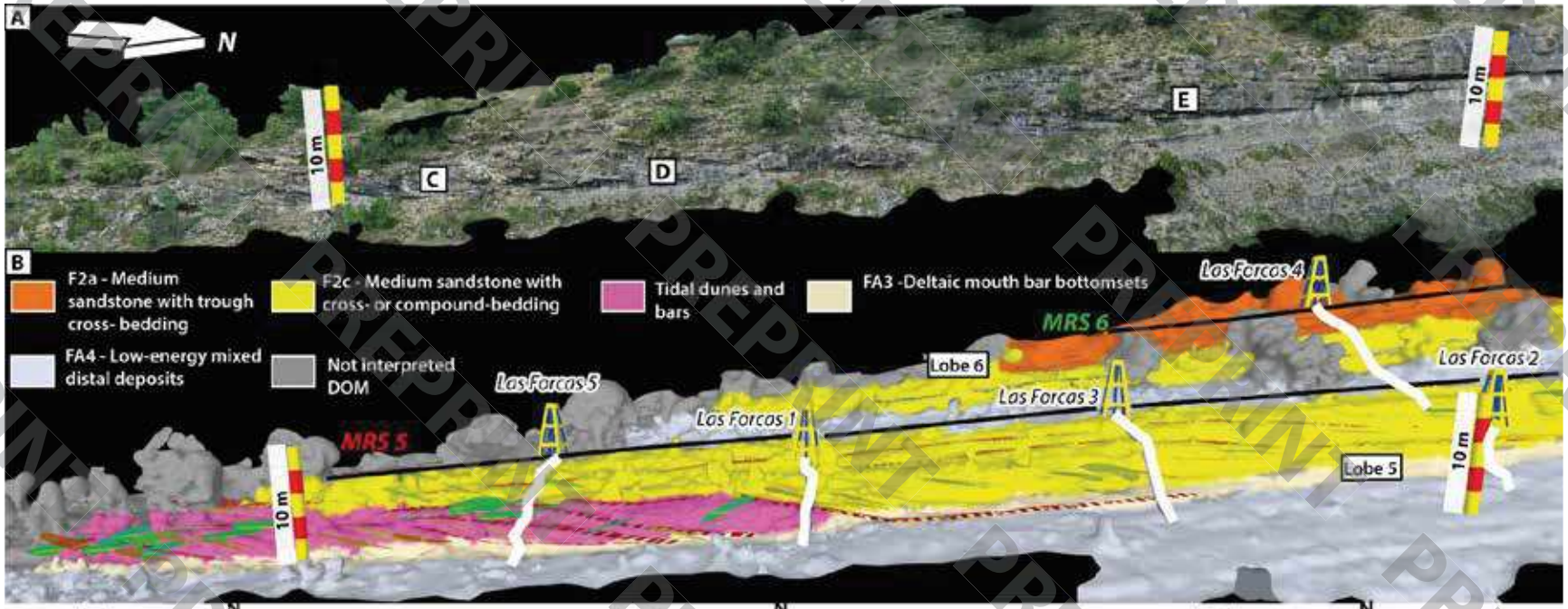


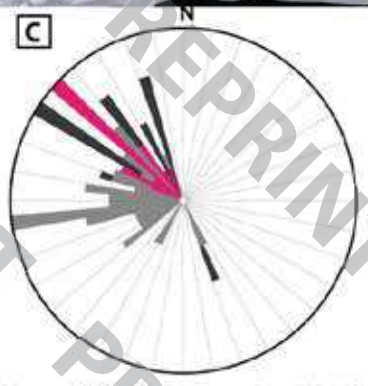


N = 14 / median azimuth = N310°
average azimuth = N310°

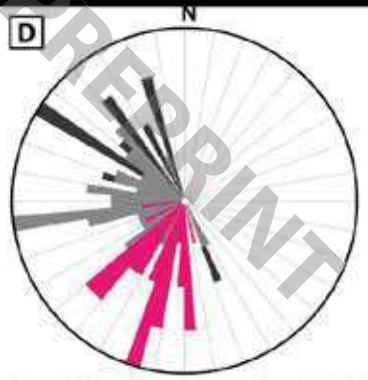


N = 28 / median azimuth = N200°
average azimuth = N205°

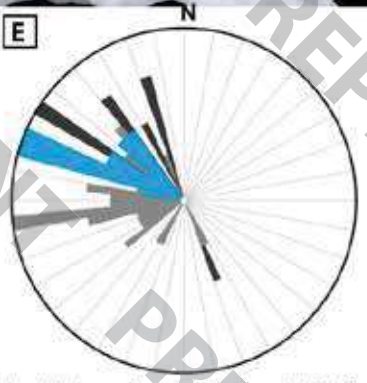


N = 20 / median azimuth = N295°
average azimuth = N300°

Figure 13

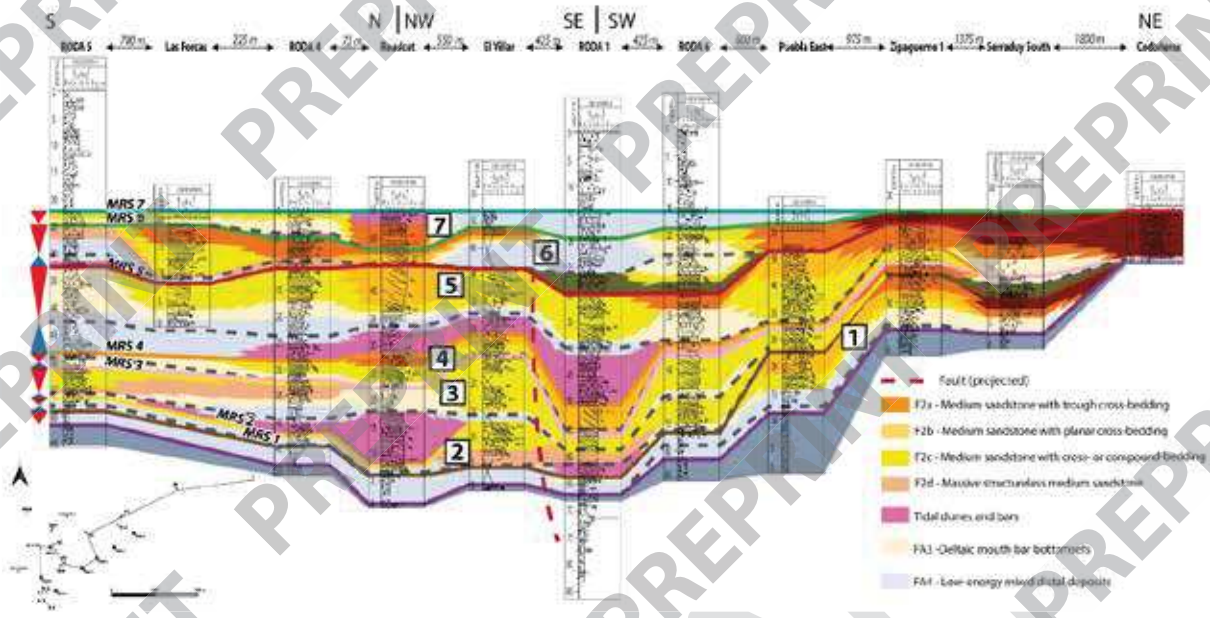


1037

1038 *Figure 14*

1039

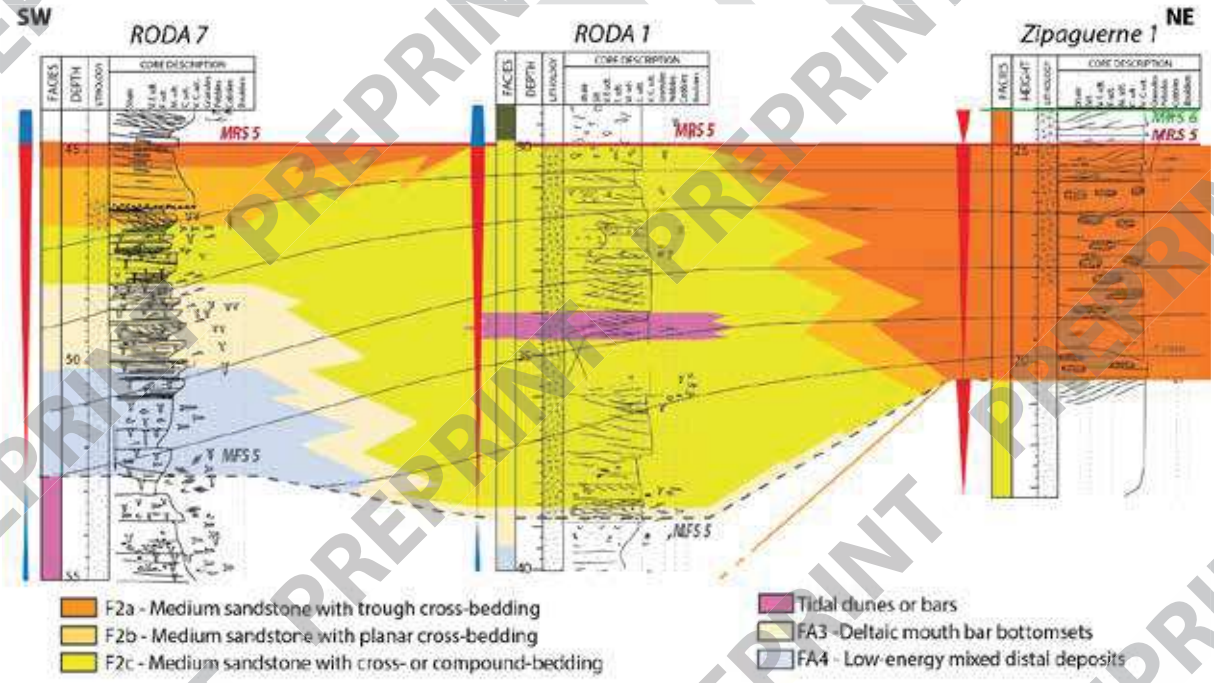


1040

1041 *Figure 15*

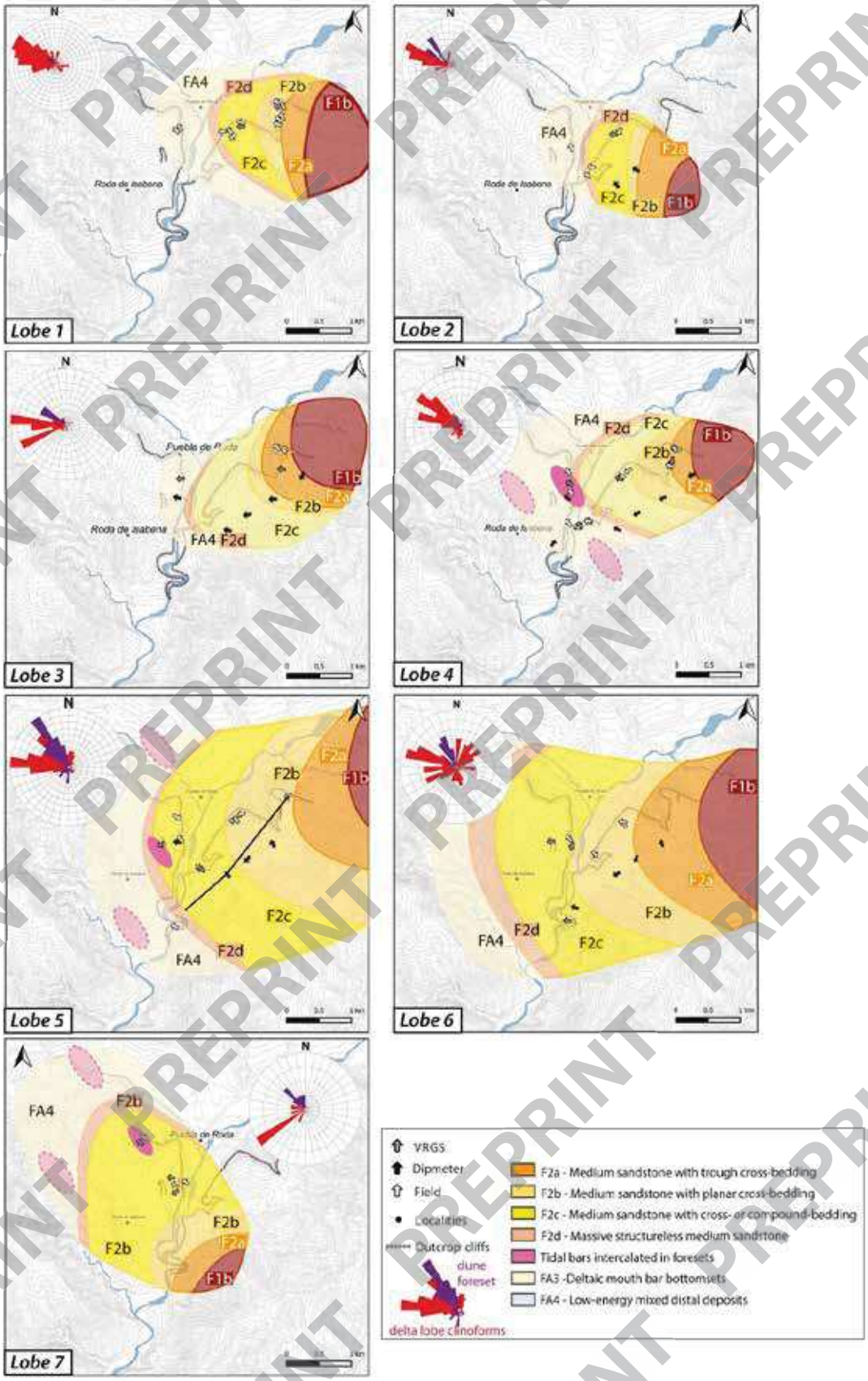


1042
1043 *Figure 16*

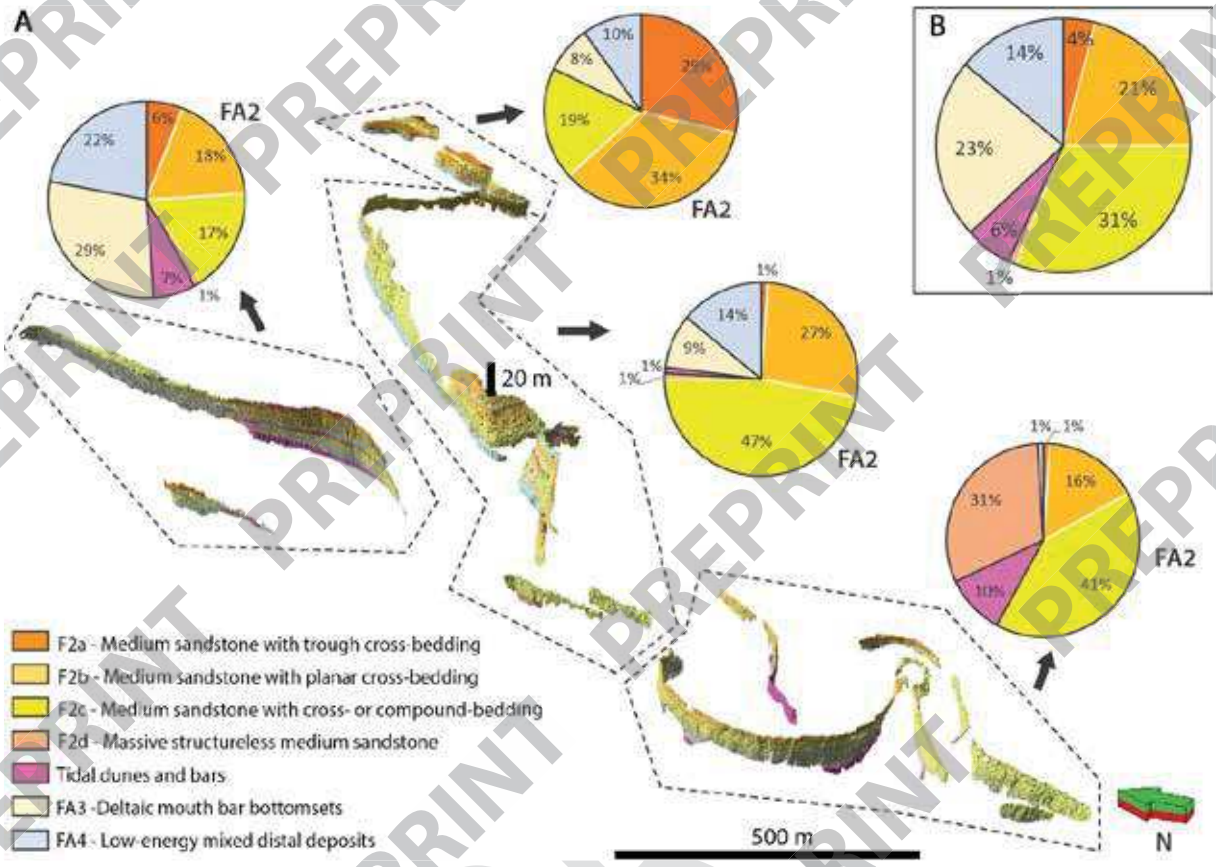


*Figure 17*

| | Length (m) | Width (m) | Max Thickness (m) |
|---|---|---|---|
| Lobe 7 | 2350 | 1500 | 10 |
| Lobe 6 | 7150 | 4680 | 25 |
| Lobe 5 | 6620 | 3610 | 30 |
| Lobe 4 | 3860 | 2220 | 15 |
| Lobe 3 | 3650 | 2230 | 10 |
| Lobe 2 | 2850 | 1860 | 20 |
| Lobe 1 | 3530 | 2360 | 25 |

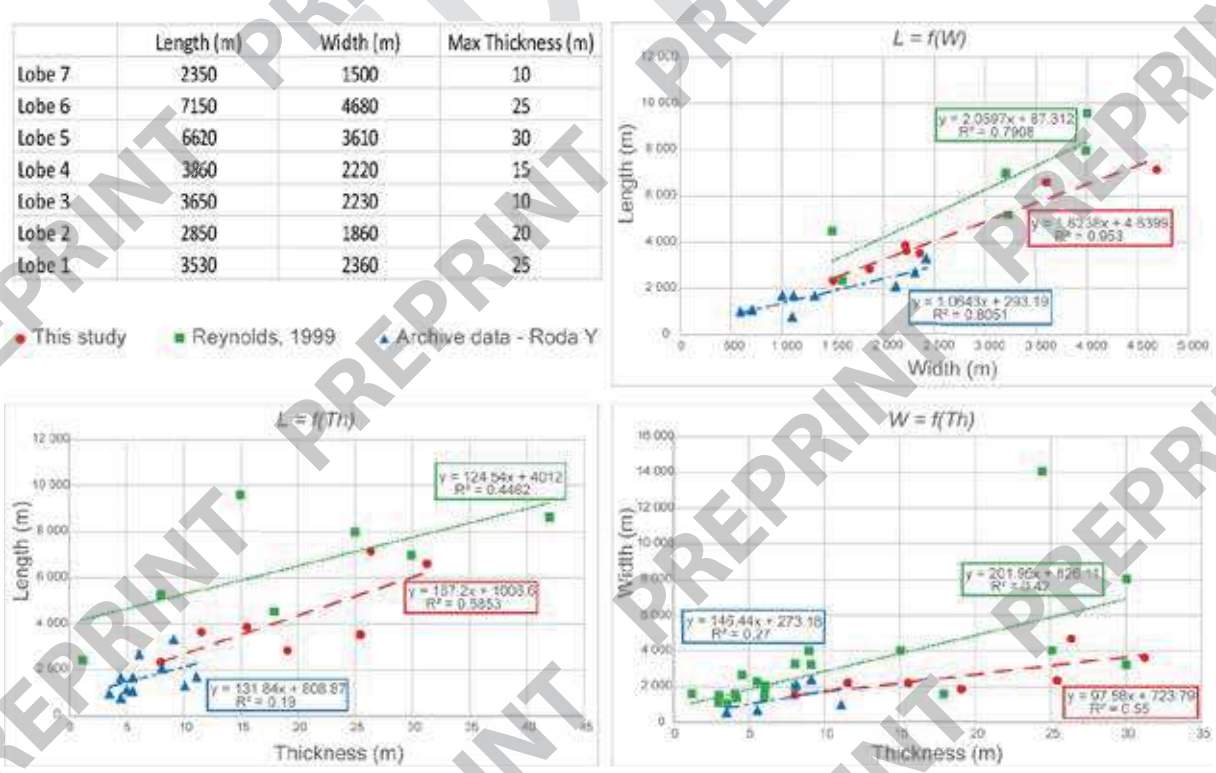


*Figure 18*

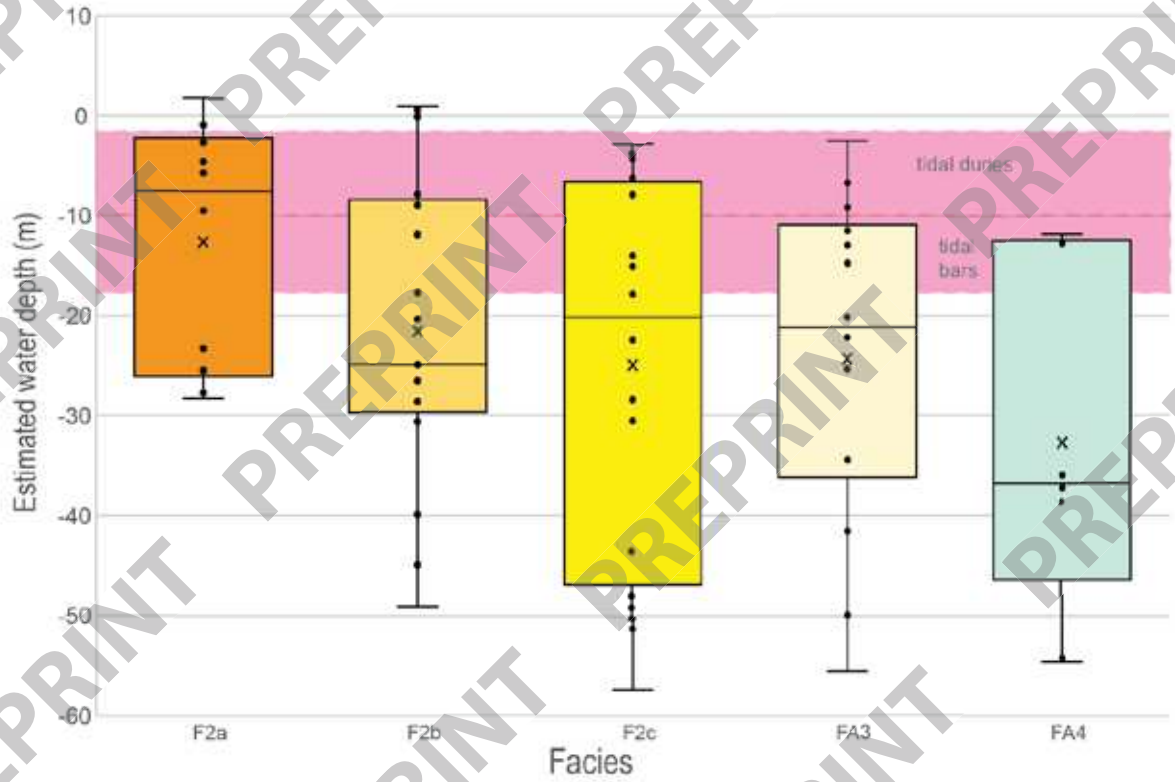


1048

1049 *Figure 19*

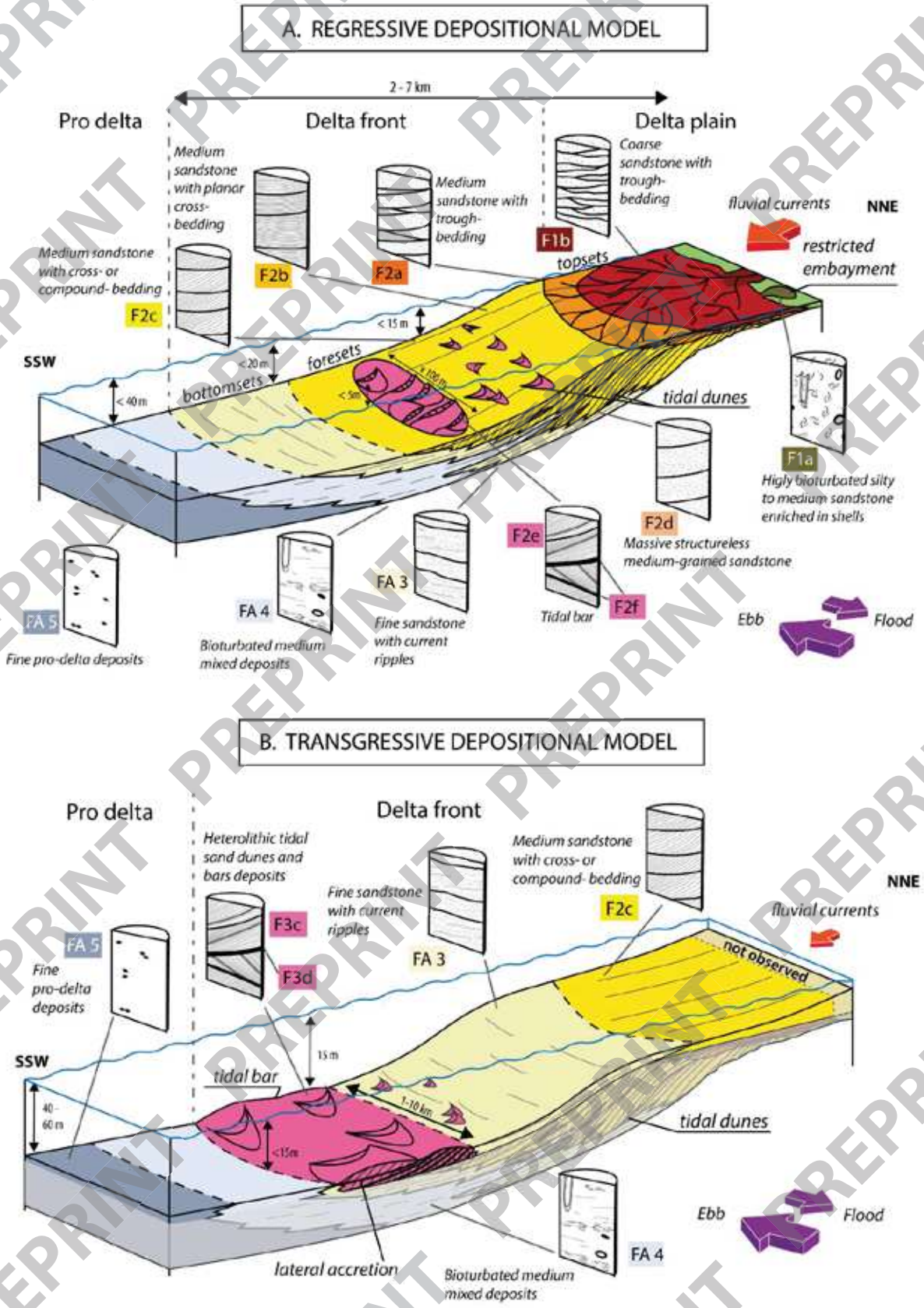


*Figure 20*

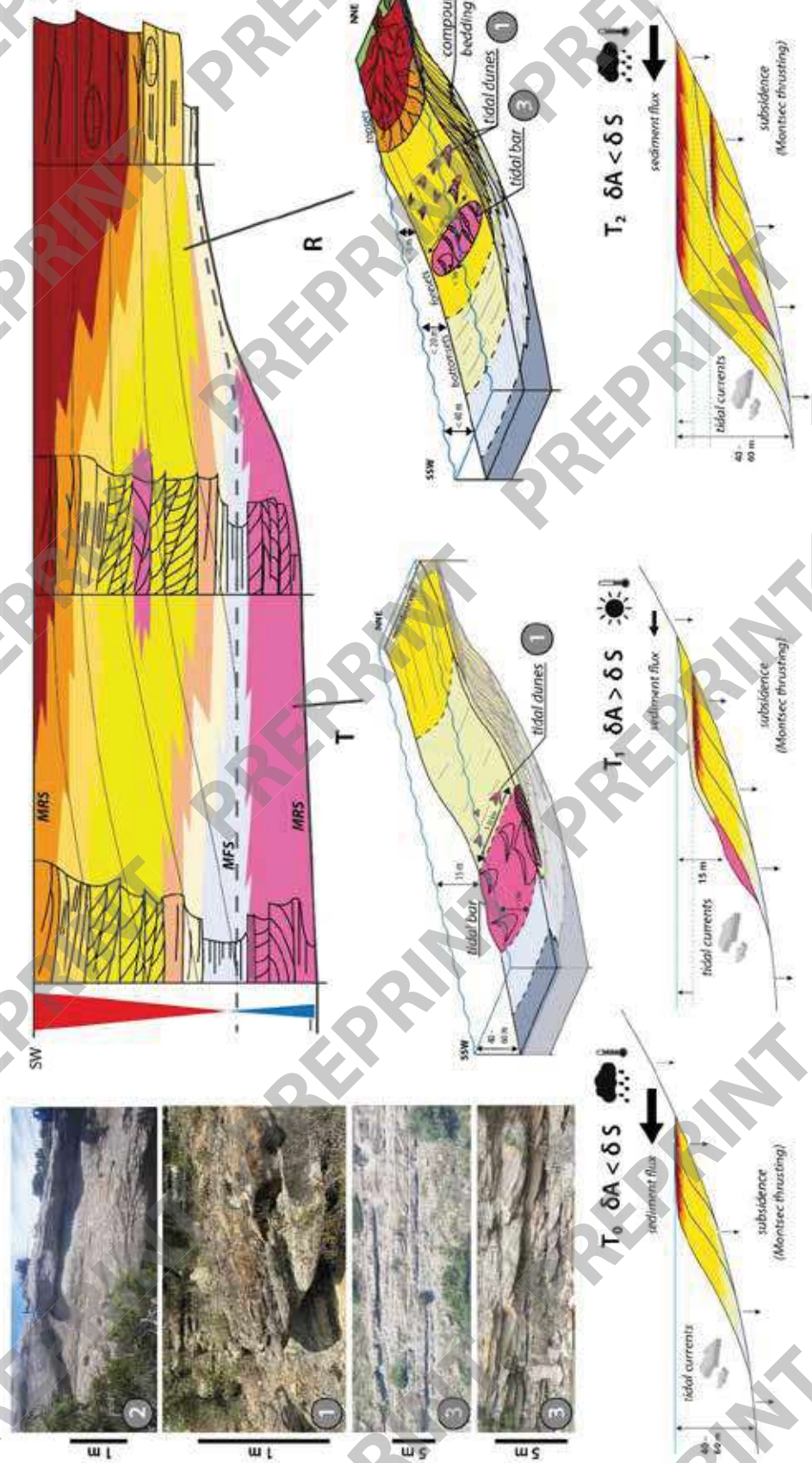


1052

1053 *Figure 21*

# 11 Supplementary Data

**Figure 22** - Cross-section 2 with lobes and facies interpretation

**Figure 23** - Cross-section 1 with lobes

**Figure 24** - Cross-section 2 with lobes

**Figure 25** - Interpreted facies on the DOM for each lobe (lobes 1 to 4)

**Figure 26** - Interpreted facies on the DOM for each lobe (lobes 5 to 7). The map on the bottom right corner depicts the facies interpretation on the DOM.

**Figure 27** – Diagram of the calculation of the water depth estimation (ΔZ_corr) of clinoforms using DOM restoration

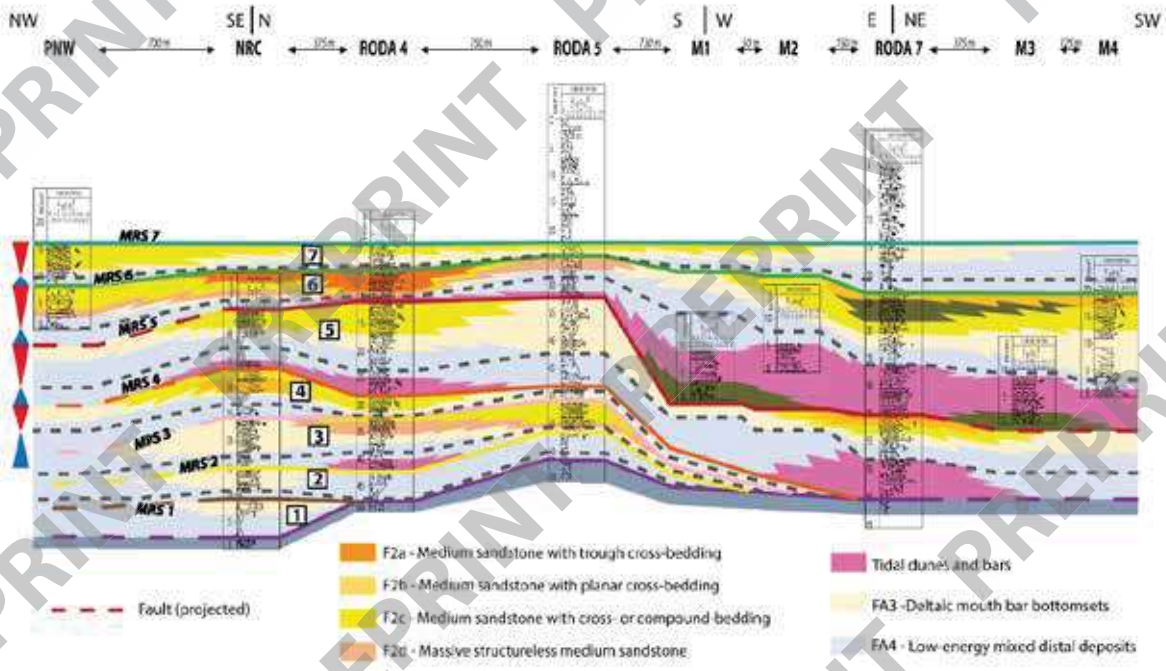


*Figure 22*

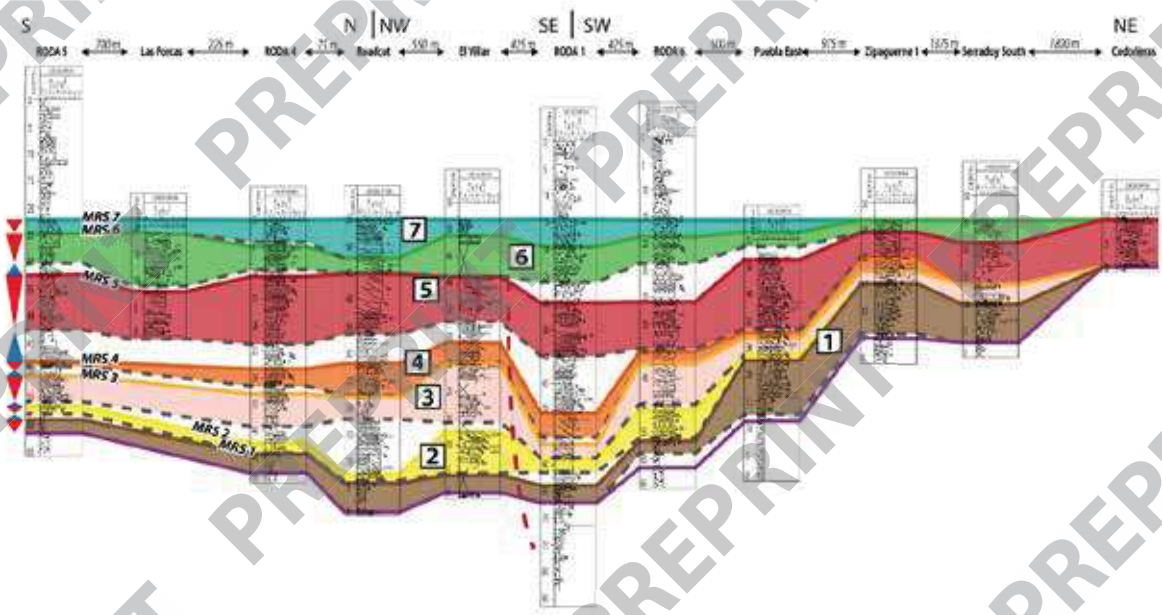


1067

1068 *Figure 23*

1069

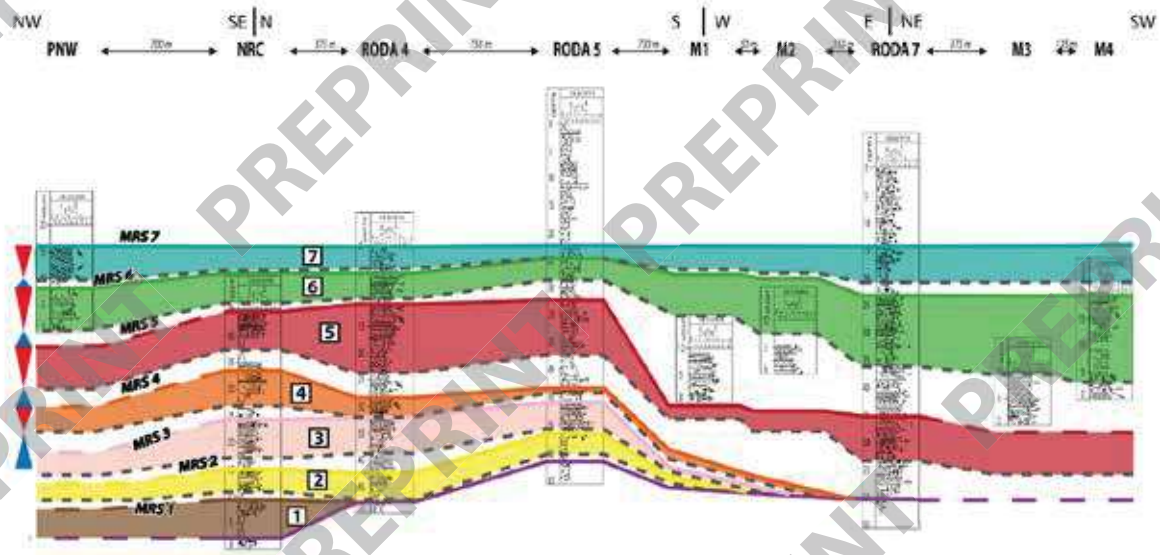


1070

1071 *Figure 24*

1072

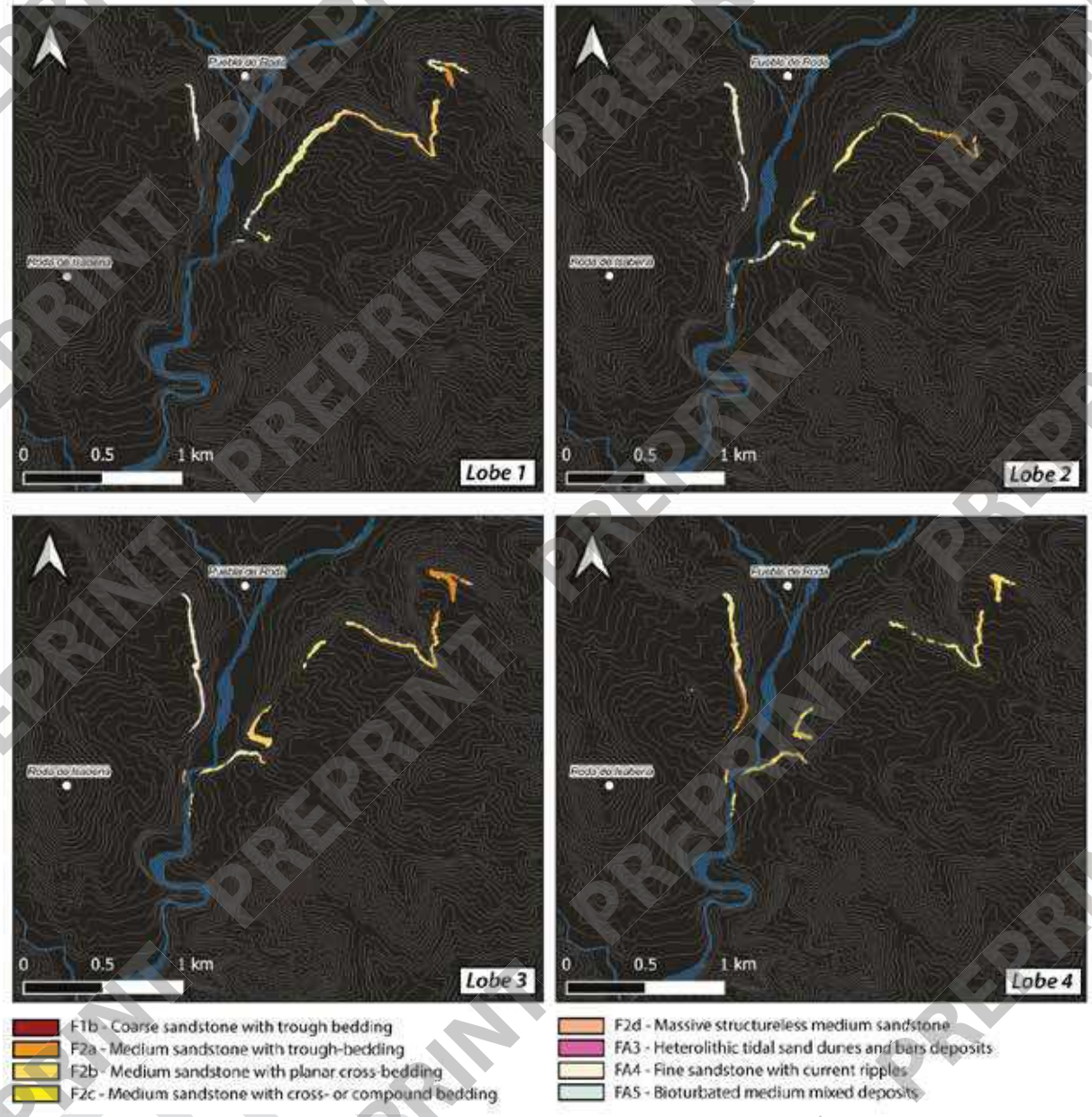


1073

1074 *Figure 25*

1075

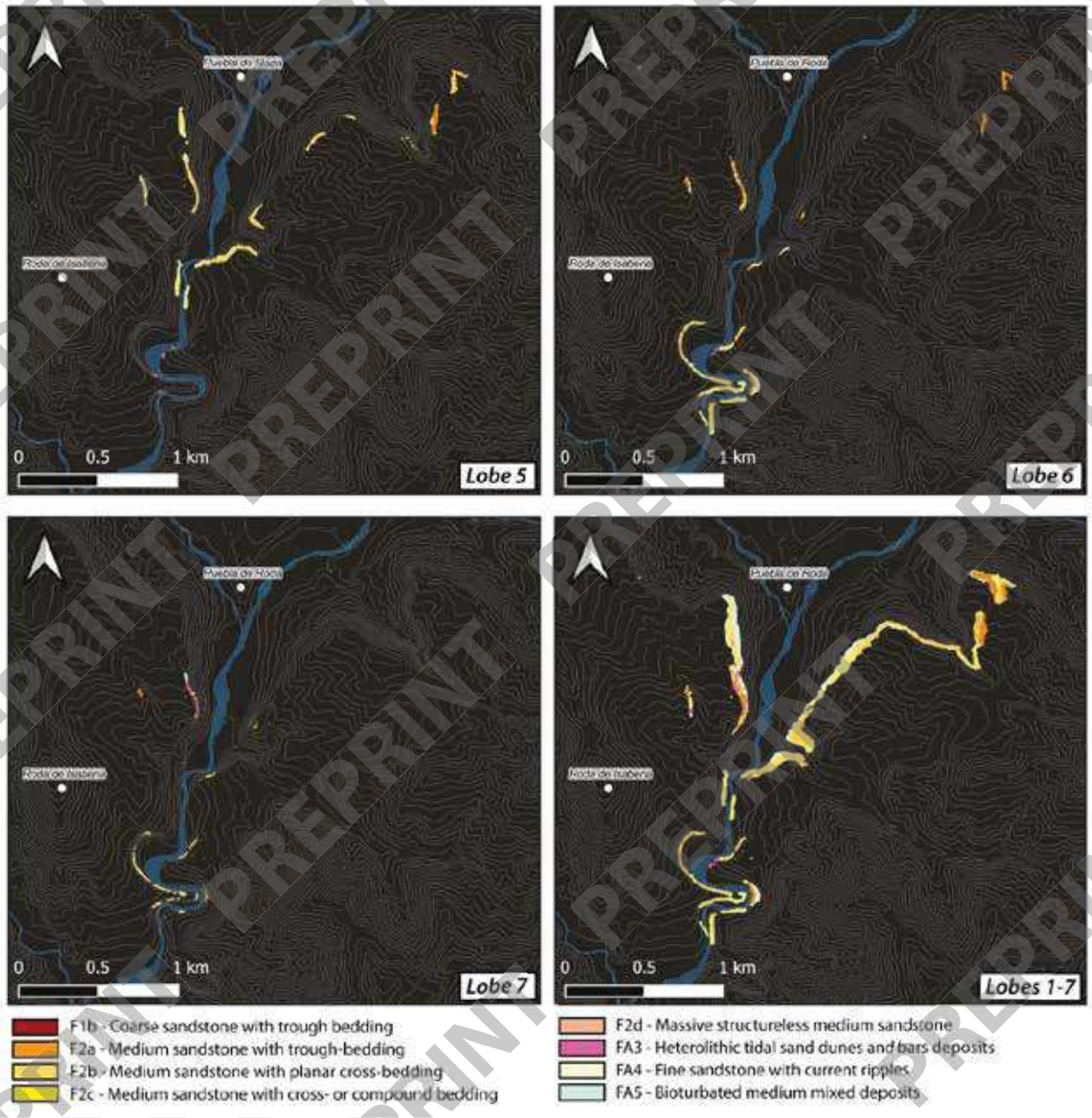


1076

1077 *Figure 26*

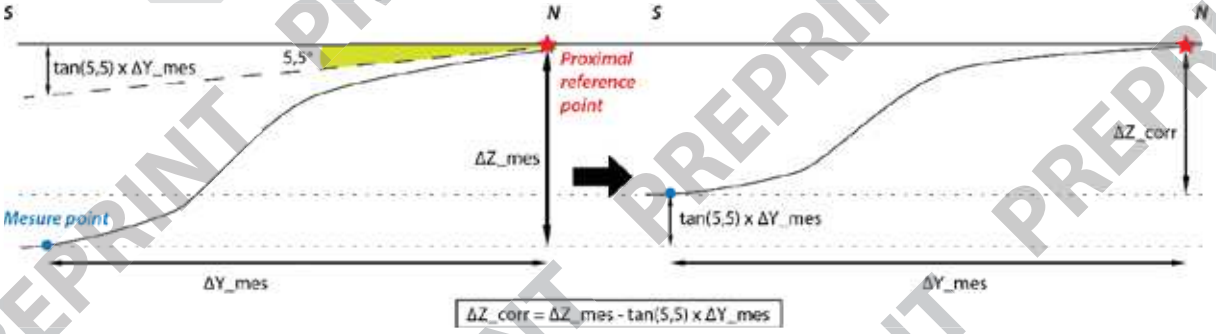


1078

1079 *Figure 27*